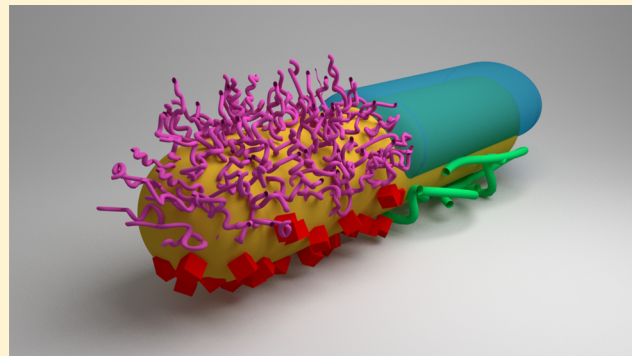


Surface Chemistry of Gold Nanorods

Nathan D. Burrows, Wayne Lin, Joshua G. Hinman, Jordan M. Dennison, Ariane M. Vartanian, Nardine S. Abadeer, Elissa M. Grzincic, Lisa M. Jacob, Ji Li, and Catherine J. Murphy*

Department of Chemistry, 600 S. Mathews Avenue, University of Illinois at Urbana–Champaign, Urbana, Illinois 61801, United States

ABSTRACT: Gold nanorods have garnered a great deal of scientific interest because of their unique optical properties, and they have the potential to greatly impact many areas of science and technology. Understanding the structure and chemical makeup of their surfaces as well as how to tailor them is of paramount importance in the development of their successful applications. This Feature Article reviews the current understanding of the surface chemistry of as-synthesized gold nanorods, methods of tailoring the surface chemistry of gold nanorods with various inorganic and organic coatings/ligands, and the techniques employed to characterize ligands on the surface of gold nanorods as well as the associated measurement challenges. Specifically, we address the challenges of determining how thick the ligand shell is, how many ligands per nanorod are present on the surface, and where the ligands are located in regiospecific and mixed-ligand systems. We conclude with an outlook on the development of the surface chemistry of gold nanorods leading to the development of a synthetic nanoparticle surface chemistry toolbox analogous to that of synthetic organic chemistry and natural product synthesis.



I. INTRODUCTION

Gold nanorods (GNRs) are well suited for a wide variety of scientific studies and technological applications because of the unique optical properties they exhibit. The demonstrated uses of GNRs include imaging,¹ biomolecular sensing,² photothermal therapy,³ and molecule delivery⁴ in biological systems. Some nonbiological applications include catalysis,⁵ sensing,⁶ and optical limiting⁷ as well as components in devices such as LEDs⁸ and solar cells.⁹

The optical properties of GNRs, like other noble metal nanoparticles, are governed by localized surface plasmon resonances (LSPRs), which are coherent oscillations of conduction band electrons in the nanoparticles in resonance with electromagnetic radiation. For noble metal nanoparticles, light in the visible region of the electromagnetic spectrum couples to LSPRs, leading to intense extinction that causes colloidal suspensions of noble metal nanoparticles to exhibit rich colors.¹⁰ Besides the material properties of the nanoparticles, the LSPR is also dependent on the effective dielectric constant of the medium surrounding the nanoparticles and on the shape of the nanoparticle. The anisotropy of GNRs allows them to support plasmons corresponding to the transverse and longitudinal dimensions of the nanorod as illustrated in Figure 1. The longitudinal resonance is particularly sensitive to the aspect ratio of the nanorod and can be tuned from the visible to the near-infrared.¹⁰ An important consequence of the LSPR is that electromagnetic fields close to the nanoparticle surface are greatly enhanced relative to the incident radiation. The strong local fields at the metal surface have been used to enhance

molecular optical processes such as fluorescence,¹¹ Raman scattering,¹² and nonlinear absorption.¹³

It is difficult to overstate the importance of surface chemical considerations when discussing GNRs. Indeed, the synthesis of anisotropic particles such as GNRs arises from subtle differences in the surface chemistry at specific crystal faces during their seed-mediated growth, the details of which are still the subject of scientific inquiry.¹⁴ Surface chemistry is also the key to the versatility of GNRs for their myriad applications. By attaching ligands to GNRs or coating them with polymers or other materials, it becomes possible to stabilize them in different chemical environments and to attach or sequester the dyes, fluorophores, and drug molecules that impart functionality to GNRs. For biological applications, it is well known that changes in nanoparticle surface chemistry can have a profound effect on cell behavior,¹⁵ gene expression,¹⁶ and cytotoxicity,¹⁷ necessitating precise control of GNR surface chemistry. As the field advances, there is an area of increasing interest in understanding how ligand arrangement varies on the surface of GNRs. Progress toward understanding the inherent anisotropy of the surface chemistry on GNRs has led to better control over site-specific modifications of GNRs,¹⁸ heralding new possibilities for the use of GNRs for catalytic purposes as well as allowing greater mastery of the synthesis and assembly of nanostructures from GNRs. In this article, we discuss the

Received: July 21, 2016

Revised: August 27, 2016

Published: August 28, 2016



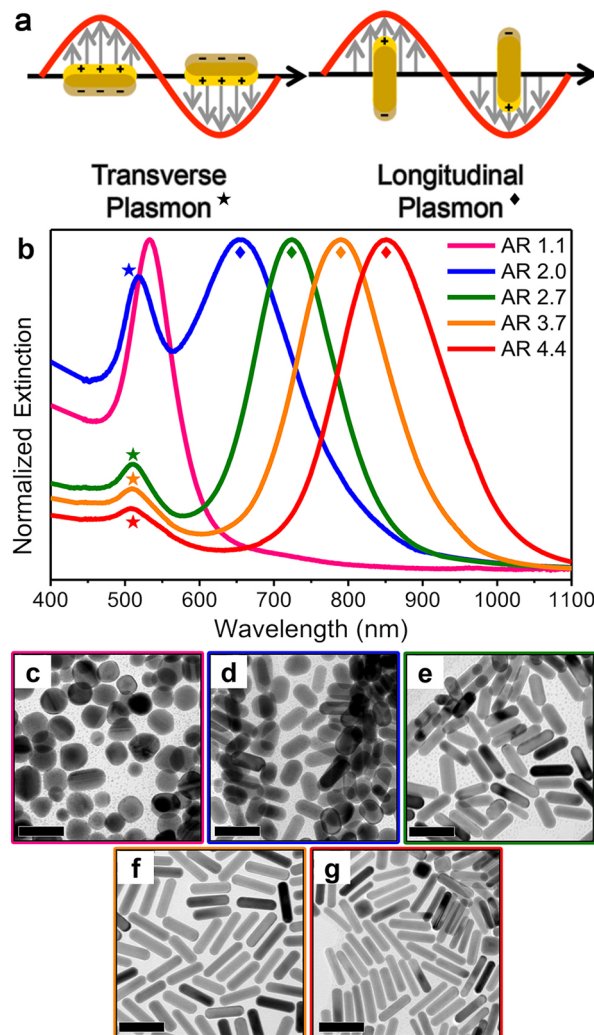


Figure 1. (a) Diagram depicting the conduction band electron oscillation (gray arrows) upon transverse and longitudinal localized surface plasmon resonances of gold nanorods. (b) Visible/near-infrared extinction spectra of gold nanorods with different aspect ratios (ARs) showing transverse (★) and longitudinal (◆) extinction peaks. TEM images of gold nanorods (c) AR 1.1, (d) AR 2.0, (e) AR 2.7, (f) AR 3.7, and (g) AR 4.4. Scale bars are 50 nm. Adapted with permission from ref 11. Copyright 2014 American Chemical Society.

surface chemistry of GNRs as well as common methods used to modify the surface chemistry, including polyelectrolyte coating, mesoporous silica coating, and covalent modifications to the GNR surface. Techniques for characterizing the surface chemistry of GNRs are also discussed, highlighting the strengths and limitations of commonly employed techniques as well as demonstrating a need for the development of new methods to better define the anisotropic arrangement of ligands on the surface of GNRs.

II. WHAT IS ON THE SURFACE?

Gold nanorods can be produced in various ways, but the seed-mediated silver-assisted gold nanorod synthesis is the most well-developed, scalable, and tunable method to date.¹⁹ The details of this method have been described in numerous other studies.^{19–27} Briefly summarized, gold nanorods are produced through the reduction of chloroauric acid by a weak reducing agent (e.g., ascorbic acid) in the presence of cetyltrimethyl-

ammonium bromide and trace silver nitrate, which is initiated by the addition of separately produced gold, small nano-spherical, crystalline seeds. The roles of silver nitrate and cetyltrimethylammonium bromide (CTAB, Figure 2) in this synthesis are unclear and have been extensively studied by many groups.^{19,28}

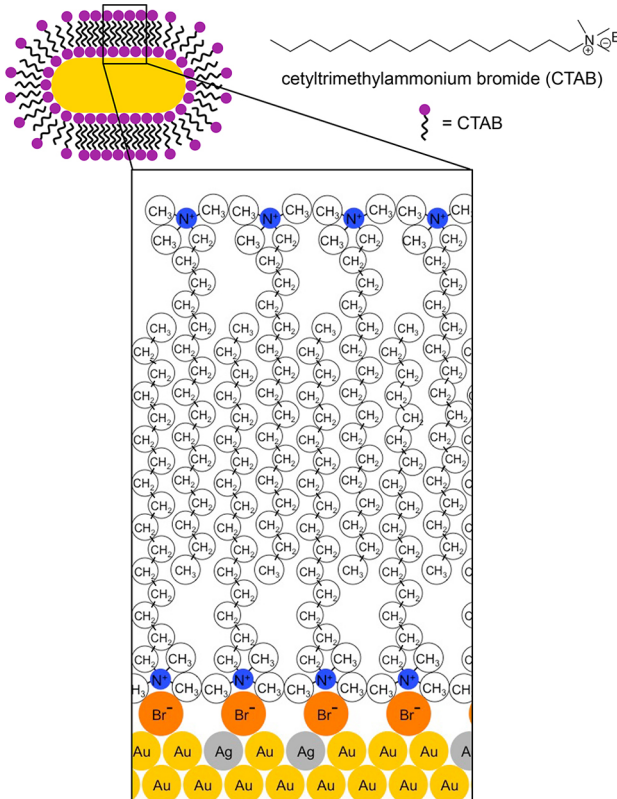


Figure 2. Structure of CTAB and its arrangement on the surface of a gold nanorod. Note that the drawing is not to scale. The inset depicts the proposed atomic-level organization of metal atoms and CTAB adsorption on the gold nanorod surface. The position of the silver atoms is not precisely known.

It is known that these gold nanorods contain silver (somewhere between 2.5 and 9%) and that it is preferentially near the surface by X-ray photoelectron spectroscopy (XPS) and Raman spectroscopy combined with inductively coupled plasma–mass spectrometry (ICP-MS).^{29,30} Recent, high-resolution transmission electron microscopy (HR-TEM) and scanning transmission electron microscopy–energy-dispersive X-ray spectroscopy (STEM-EDX) maps have shown the presence of silver at the surface of all faces of GNRs.³¹ Extended X-ray absorption fine structure (EXAFS) analysis of photochemically synthesized gold nanorods indicates the presence of Ag^0 at the surface but shows no contribution from AgBr or Ag^+ at all.³² However, many pieces of evidence point to the existence of Ag–Br complexes as well when gold nanorods are produced using aqueous redox chemistry instead of photochemical reduction. XPS and Raman spectroscopy have been used to show the influence of Au–Br and Ag–Br species, and one study has shown that the Au–Br Raman band disappears upon addition of thiols.^{30,33–35} Using mass spectrometry, Niidome et al. have shown the presence of AgBr^{2-} and AuBr^{2-} on the surface of gold nanorods.³⁶ Complementary XPS and quartz crystal microbalance (QCM)

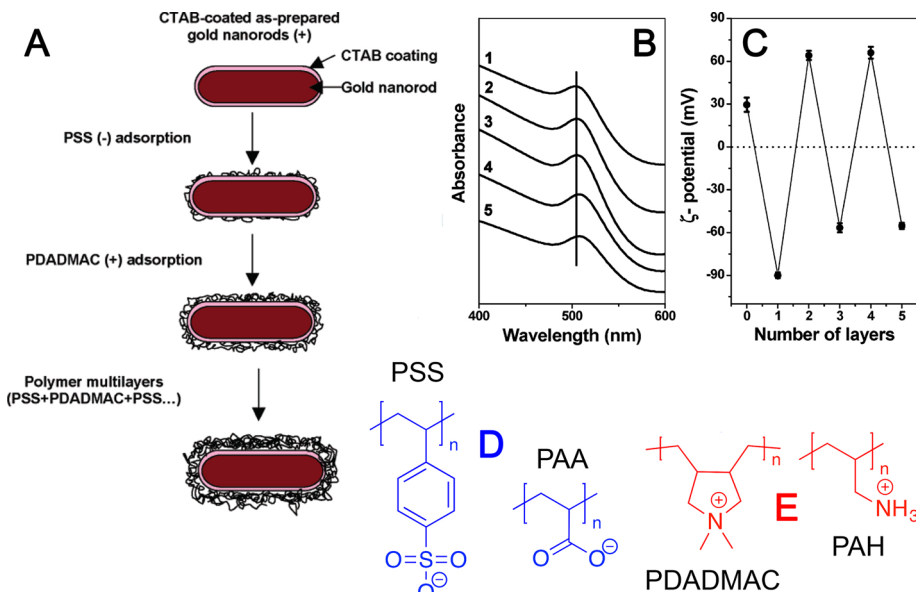


Figure 3. (A) Schematic diagram illustrating the layer-by-layer (LbL) coating process of gold nanorods. (B) Visible spectra of gold nanorods as a function of polymer coatings: (1) Uncoated as-prepared GNR, (2) one polymer layer (PSS), (3) two polymer layers (PSS + PDADMAC), (4) three polymer layers (PSS + PDADMAC + PSS), and (5) four polymer layers (PSS + PDADMAC + PSS + PDADMAC). Curves are offset for clarity. (C) Zeta potential data for gold nanorods as a function of polymer coatings. Common (D) anionic (blue) and (E) cationic (red) polyelectrolytes used for layer-by-layer assembly to achieve gold nanorod functionalization at pH 7. Panels A–C are adapted with permission from ref 50. Copyright 2005 American Chemical Society.

measurements) performed on gold surfaces indicate that an Ag–Br–CTA complex adsorbs to gold much more strongly than CTAB (and other halide-CTAs) alone, and nuclear magnetic resonance (NMR) and Fourier transform infrared spectroscopy (FTIR) spectra of Ag–Br–CTA show strong similarities to the spectra of CTAB-nanorods.³³ The role of the bromide ion is important: under the same conditions, CTA-Cl cannot be used to replace CTA-Br completely, though it can be done with CTAB-coated gold seeds and sodium oleate.³⁷ However, the CTA⁺ concentration can be reduced by a factor of 2 by replacing lost bromide ions with salt.^{38,39} The role of halides in the synthesis of anisotropic metal nanoparticles has been discussed in further detail in a recent perspective article.⁴⁰

Regardless of the location and chemical state of the silver, it is generally well accepted that CTAB is present on the surface of completed nanorods as a bilayer, through electrostatic interactions of the ammonium headgroup and an anionic nanorod surface consisting of metal bromide complexes (Figure 2).^{19,41} FTIR and thermogravimetric analysis (TGA) experiments by Nikoobakht et al. indicate that there are CTAB molecules in two different environments—one with head groups near the gold surface in an inner layer and one with headgroups toward the environment in an outer layer—and that the long hydrocarbon chains are packed together.⁴² Small-angle X-ray scattering (SAXS) and small-angle neutron scattering (SANS) have shown a bilayer thickness of 32 ± 2 Å, which shows that the bilayer is potentially interdigitated.⁴³ Another recent study using SAXS determined that very little exchange happens between surfactant on the original seed particles and surfactant in the growth solution and that using CTA-Cl rather than CTAB in the growth solution does not alter the bilayer structure.⁴⁴ However, the diffusion of individual CTAB molecules along the GNR surface is to be expected, in a manner similar to how molecules can diffuse across a flat surface.^{45,46} Given the increased radius of curvature of a GNR,

one would expect increased mobility of surface ligands on a GNR surface when compared to that on a flat surface, but to our knowledge, there have not been any studies documenting this phenomenon on GNRs. Nevertheless, the CTAB bilayer provides a stable platform to further physiochemically modify the surface in the pursuit of various applications.

III. MODIFYING THE SURFACE

Many of the applications highlighted in the **Introduction** are possible only through understanding and manipulating the surfaces of gold nanorods. With knowledge of the as-synthesized chemical nature of the GNR surface (discussed in the previous section), researchers have devised many approaches to tune the surface chemistry of gold nanorods, often with multiple routes of achieving the same goals. For example, gold nanorods are synthesized under aqueous conditions; however, it may be advantageous to transfer the nanorods to another polar solvent or phase that is not compatible with water while maintaining a well-dispersed and stable colloidal suspension. The phase transfer of gold nanoparticles to nonaqueous solvents has been achieved by manipulating the hydrophilicity of the nanoparticle surface through layer-by-layer polyelectrolyte wrapping,⁴⁷ coating with hard inorganic shells (e.g., silica),¹¹ and covalent modification through gold–thiol chemistry.^{48,49} In the following subsections, we discuss the multitude of methods for modifying the surface chemistry of gold nanorods.

III.A. Polyelectrolyte Coating. One straightforward approach to modifying the surface employs the large positive charge of the CTAB bilayer by depositing charged polyelectrolytes (PE) on the GNR surface. By alternatively adding PEs of opposite charge (e.g., negatively charged poly(sodium-4-styrenesulfonate) (PSS) and positively charged poly(diallyldimethylammonium chloride) (PDADMAC) (Figure 3)), a layer-by-layer (LBL) assembly of PEs can be built to

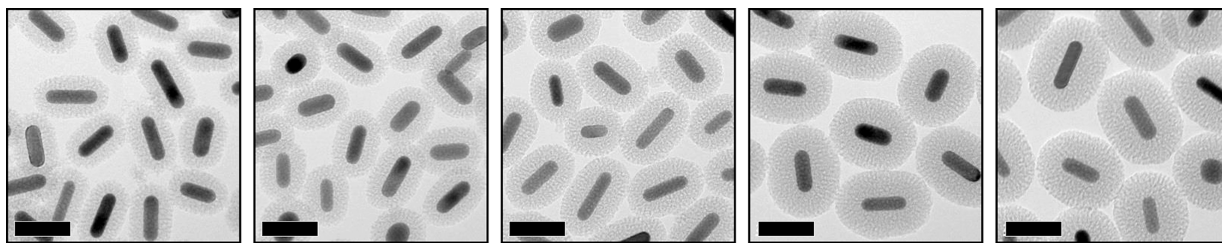


Figure 4. Transmission electron microscopy images of aspect ratio 2.7 mesoporous silica-coated gold nanorods with shells 11, 14, 17, 22, and 26 nm thick from left to right. Scale bars represent 50 nm. Adapted with permission from ref 11. Copyright 2014 American Chemical Society.

achieve polymer multilayers on the GNR surface.⁵⁰ Successful LBL assembly of PEs on gold nanorods is dependent on a balance between the ionic strength and the polymer molecular weight. This is to screen intra- and intermolecular electrostatic repulsions so that the polyelectrolytes are in a flexible, extended conformation for wrapping without causing flocculation due to insufficient electrostatic repulsion, lack of coating due to polymer rigidity, and multimer formation through polymer bridging between nanorods. Another key factor is sufficient time for the large polymer macromolecules to diffuse and wrap the gold nanorods; in other words, the coating process can be slow.

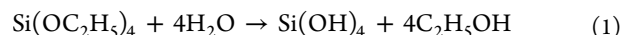
One advantage of the LBL coating method, besides the simple procedure, is that the surface charge can be easily varied on the basis of the choices of PE layers. Hauck et al. applied PSS, PDADMAC, and poly(allylamine hydrochloride) (PAH) to synthesize four different PE-coated GNRs with different charge, number of layers, and composition to test their effect on GNR cellular uptake, toxicity, and gene expression.⁵¹ The tunable uptake and toxicity of PE-wrapped GNRs shows the advantage of this method in fine-tuning GNR properties for potential biomedical applications. Poly(acrylic acid) (PAA) and PAH-coated GNRs of varying aspect ratios have also been prepared for a cellular uptake study, and it was found that the toxicity of GNRs was significantly reduced after PE coating as a result of the covering up of CTAB.⁵² It has also been demonstrated that LBL PE-coated GNRs strongly adsorb proteins and thus can influence cell function.^{16,53}

Layer-by-layer polyelectrolyte GNR surface functionalization allows for straightforward loading of molecules on or within the PE multilayers based on electrostatic interactions. Ni et al. applied this method to load a positively charged dye on PSS-coated GNRs.⁵⁴ Gandra et al. applied PEs as dielectric spacers on immobilized GNRs and probed distance-dependent plasmon-enhanced fluorescence with a fluorophore adsorbed on the outer PAH layer.⁵⁵ Similar small-molecule loadings have also been done with organic chromophores to study the GNR surface plasmon enhancement of the molecule's two photon absorption cross section¹³ and SERS probes for the observation of molecular diffusion within the PE layers.⁵⁶ It has been shown that molecules electrostatically loaded within the multilayers can be released through a photothermal mechanism for a controllable release based on the number of PE layers.⁵⁷ Macromolecules such as antibodies have also been electrostatically attached to PEs⁵⁸ or covalently attached to the carboxyl group of PAA^{59,60} to provide an active targeting capability for imaging and therapeutic applications.

III.B. Mesoporous Silica Coating. Numerous reports exist on the synthesis and application of gold nanorods coated with mesoporous silica.^{11,61,62} Silica coating can improve the colloidal and thermal stability of gold nanorods in organic

solvents while preserving their unique optical properties.¹¹ The presence of reactive silanol groups on a silica surface is very useful for additional surface modification of gold nanorods with molecules such as biocompatible polymer poly(ethylene glycol), the loading of chemotherapeutic drugs, or the attachment of targeting ligands for biological applications.^{63,64} Also, silica can act as a dielectric layer to investigate distance-dependent molecular responses in fluorescence emission or Raman intensity near a plasmonic surface.^{11,65} Therefore, the achievement of robust and reproducible growth of silica shells on gold nanorods is a key one for future applications.

Mesoporous silica nanoparticles contain hexagonally ordered pores with uniform sizes, and the pores are typically 0.5–3 nm in diameter.⁶⁶ The Stöber process is the basis for the mesoporous silica coating on inorganic nanoparticles. Stöber was able to achieve controlled synthesis of silica spheres 0.05–2 μm in diameter through the hydrolysis and condensation of tetraalkyl silicates at pH 11–12 (eqs 1 and 2).^{67,68} Mesoporous silica is synthesized by reproducing the Stöber method in the presence of a surfactant, such as CTAB, which forms a template of ordered micelles.⁶⁹ Nooney et al. proposed that mesoporous silica formation on gold nanoparticles occurs in three stages: (1) hydrolysis and condensation resulting in the formation of silica oligomers, (2) formation of primary silica/CTAB particles, and (3) deposition of the primary particles on silica or CTAB.⁷⁰ Therefore, parameters such as the CTAB concentration, pH, and reaction temperature can be modified to control the mesopore structure and size of nanoparticles formed.⁶⁹



Gorelikov et al. adapted the Stöber procedure and were among the first to directly coat mesoporous silica onto aspect ratio 1–5 CTAB gold nanorods.⁶² In their procedure, NaOH is added to concentrated gold nanorods to adjust the pH to 11. This is followed by injections of tetraethylorthosilicate (TEOS) that polymerizes to form silica in a base-catalyzed reaction. With this simple method, they produced 15-nm-thick silica shells. Furthermore, 60-nm-thick nonporous silica shells were prepared by injecting additional TEOS into the reaction solution after the initial coating.⁶²

The controlled growth of mesoporous silica on gold is a complicated process because the silica shell morphology is dictated by the surfactant template and the CTAB/silica ratio. As a quaternary ammonium surfactant, CTAB exhibits concentration-dependent micelle behavior.⁷¹ Our group has demonstrated that one of the most important parameters in mesoporous silica shell formation on gold nanorods is the external CTAB concentration.¹¹ As-synthesized gold nanorods

are typically prepared in 0.1 M CTAB, but after purification via centrifugation and resuspension in water, the concentration of CTAB can vary. The critical micelle concentration (CMC) of CTAB is ~ 1 mM in pure water, 2 orders of magnitude lower in concentration than the original synthesis conditions.⁷² In our preparation, we carefully control the CTAB concentration during silica coating. The CTAB concentration is reduced via additional centrifugation and removal of the supernatant solution above the gold nanorod pellet. We estimate that this reduces the CTAB concentration to <0.01 mM, and then a known amount of CTAB is added to adjust the concentration to 0.4–1.2 mM. Subsequent adjustment of the pH and addition of TEOS resulted in the formation of mesoporous silica shells between 11 and 26 nm thick, depending on the external CTAB concentration present (Figure 4). By adjusting the CTAB concentration closer to the CMC (0.4–1.2 mM), we find that it is possible to form mesoporous silica shells on gold nanorods. We propose that at lower CTAB concentrations the majority of CTAB is on the surface of the gold nanorods, resulting in the formation of thicker silica shells.¹¹ When the CTAB concentration is increased, more silica forms around free CTAB in solution and results in thinner silica shells on the gold nanorods. When the concentration of CTAB is much higher than the CMC, silica forms only around free CTAB micelles and not the gold nanorods. Therefore, control of silica shell thickness is achieved by controlling the CTAB concentration.¹¹

Other researchers have altered the morphology of mesoporous silica on gold nanorods using different methods. For example, Cong et al. controlled the shell thickness from 60–150 nm by varying the TEOS concentration during coating.⁷³ Wu et al. added PEG-silane at various time points after the TEOS addition, which terminated silica growth. With this method, they controlled the shell thickness to between 2 and 9 nm. The same group also demonstrated control between 3 and 17 nm by adjusting the TEOS concentration.⁶⁴ Liu et al. used chiral anionic surfactants (*N*-palmitoyl-L,D-phenylalanine) with costructure directing agent *N*-((trimethoxysilyl)propyl)-*N,N,N*-trimethylammonium chloride instead of CTAB. This produced chiral porous shells 9–45 nm thick that preferentially adsorbed chiral cysteine molecules of a matching chirality, where chirality was confirmed using circular dichroism and pore selectivity was confirmed via new vibrational bands.⁷⁴

Wang and co-workers recently reported site-selective side and end mesoporous silica coatings of gold nanorods (Figure 5).⁷⁵ In their procedure, CTAB and TEOS are carefully controlled to allow the preferential deposition of silica on the nanorod ends. The addition of a PEG-thiol to selectively functionalize the nanorod ends allowed for the formation of side silica-coated nanorods.⁷⁵ In addition to the shell thickness, it may also be possible to adjust the reaction parameters to control the mesopore structure in mesoporous silica-coated gold nanorods.⁶⁹

The porosity of mesoporous silica is dependent on a variety of factors, and there are a few examples of pore characterization on mesoporous silica-coated gold nanorods in the literature. These values are summarized in Table 1. The silica surface area, pore volume, and pore diameter do appear to vary among the different nanoparticle systems. However, because the nanorod dimensions and silica shell thicknesses vary, it is difficult to ascertain which synthesis parameters are the most critical to mesopore morphology. Nevertheless, these reports demonstrate that this modified Stöber process is quite versatile in the morphology and thickness of mesoporous silica that can be

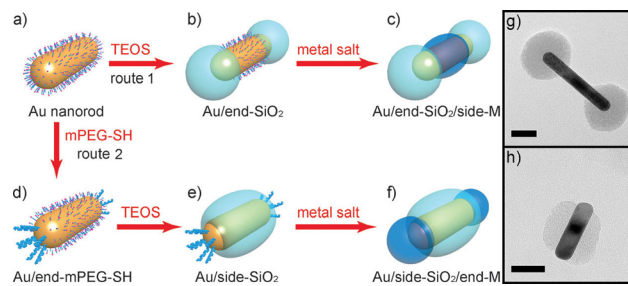


Figure 5. Routes of side and end silica coatings as evidenced by metal overgrowth. (a) Gold nanorod capped with a CTAB bilayer. (b) Gold nanorod coated with silica at the ends. (c) Gold nanorod overgrown with a metal on the side surface. (d) Gold nanorod bonded with mPEG-SH on the ends. (e) Gold nanorod coated with silica on the side surface. (f) Gold nanorod overgrown with a metal at the ends. Adapted with permission from ref 75. Copyright 2013 John Wiley and Sons. In (g) and (h) are TEM images showing gold nanorods prepared in our laboratory following protocols adapted from ref 75 with silica at the ends and side surface, respectively. Scale bars are 25 nm.

formed on gold nanorods. This is especially useful when considering applications of silica-coated gold nanorods.

III.C. Thiol Modification. Ligand exchange, depicted schematically in Figure 6, is one of the most versatile methods used to tailor the surface chemistry of GNRs. Importantly, the cytotoxicity of the CTAB used to synthesize GNRs⁵² makes ligand exchange especially useful when GNRs are used for biological applications. For an in-depth discussion of ligand exchange on gold nanorods, we refer the reader to the progress report by Indrasekara et al.⁷⁹ Although any ligand capable of displacing CTAB can be used for ligand exchange, alkanethiols are some of the most commonly used molecules for ligand exchange on gold nanoparticles. Many factors affect ligand exchange and contribute to the characteristics of the resulting mixture of ligands on the nanoparticle including ligand–surface interactions, ligand–ligand interactions, ligand–solvent interactions, and particle morphology,^{79–81} but the relatively strong gold–thiolate bond (~ 44 kcal/mol)⁸² makes alkanethiols particularly useful for ligand exchanges. Gold–alkanethiolate self-assembled monolayers (SAMs) have been extensively studied on flat gold surfaces. On gold {111} surfaces, alkanethiolate SAMs chemisorb with a $(\sqrt{3} \times \sqrt{3})R30^\circ$ arrangement and a 28° cant angle.⁸³ It is more difficult to directly measure the structure of alkanethiolate SAMs on gold nanoparticle surfaces, but the high curvature of gold nanoparticle surfaces likely allows greater flexibility at the distal ends of the alkanethiolate molecules. Experimental measurements indicate that the density of alkanethiolate molecules is greater on nanoparticles than on flat surfaces,⁸⁴ and simulations suggest that the organization of SAMs on nanoparticle surfaces is dependent on particle shape.⁸⁵ As has been reviewed elsewhere, thiolated molecules can be functionalized using myriad chemistries such that a host of biomolecules, dyes, reporters, and other molecules can be conjugated to gold nanorod surfaces through ligand exchange.⁸⁶ The range of surface chemistries that can impart functionality to gold nanorods and stabilize them in many different solvents and systems made available via thiolate ligand exchange contributes to the tractability of nanorods for many different applications.

The hydrophobic nature of many alkanethiols can present some challenges for performing successful ligand exchanges. The direct replacement of CTAB on GNRs by thiolated ligands

Table 1. Reported Values of Surface Area and Pore Diameter on Mesoporous Silica-Coated Gold Nanorods

reference	nanorod dimensions	shell thickness	BET surface area	total pore volume	pore diameter
Sanz-Ortiz ⁷⁶	—	—	—	—	2.1 nm
Tang ⁷⁷	10 nm × 45 nm	—	328 m ² /g	0.64 cm ³ /g	2.8 nm
Shen ⁷⁸	13 nm × 52 nm	25 nm	348 m ² /g	0.51 cm ³ /g	2.9 nm
Liu ⁷⁴	45 nm × 70 nm	15 nm	75 m ² /g	—	2.9 nm
Gorelikov ⁶²	10 nm × 35 nm	15 nm	—	—	~4 nm

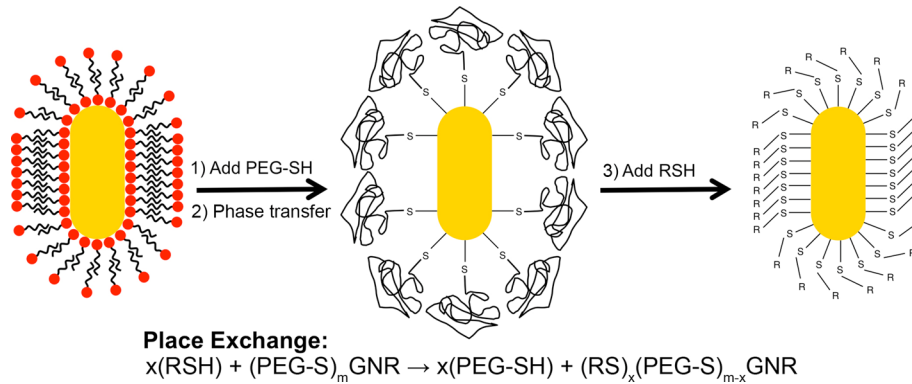


Figure 6. Schematic representation of the ligand exchange of CTAB for PEG-SH followed by the place exchange of PEG-SH for an alkanethiol. The reaction for the place exchange is also shown. Replacing CTAB with PEG-SH provides a facile means of transferring the GNRs into an organic phase to functionalize the surface with RSH without causing particle aggregation. Images are not drawn to scale.

can often lead to the aggregation of the GNRs. As discussed by Indrasekara et al., different strategies of ligand exchange such as one-pot ligand exchange, phase transfer, and solid-phase ligand exchange have been developed to address the unique problems associated with the exchange of certain ligands for different applications.⁷⁹ An effective method that has proven useful in our laboratory to address some of the challenges of functionalizing GNRs with thiols involves the functionalization of CTAB-capped GNRs by poly(ethylene glycol) methyl ether thiol (PEG-SH) with a molecular weight of 1–10 kDa, phase transfer of the PEGylated GNRs to a suitable solvent, and finally ligand exchange of the PEG-SH for the desired small molecule thiol.⁸⁷ For the functionalization of GNRs by PEG-SH, excess CTAB is removed (often by centrifugation), and then PEG-SH is added to the GNRs in aqueous solution and given time to attach to the GNR surface.⁴⁷ The PEG-SH-functionalized GNRs can then be resuspended in organic solvent after centrifugation. The phase transfer of PEG-SH-functionalized GNRs from an aqueous phase to an immiscible organic phase may also be accomplished by the mechanical force of centrifugation,⁸⁸ or centrifugation may be avoided entirely through the use of a common solvent that is miscible in both aqueous and organic phases.⁴⁸ Although small-molecule thiols can serve to facilitate the phase transfer of gold nanoparticles from the aqueous to the organic phase, it can be difficult to achieve without aggregation. Because the exchange of CTAB for PEG-SH can be done in the aqueous phase, it is often easier to use PEG-SH-functionalized nanorods for phase transfer without inducing aggregation.

Once the GNRs are in the organic phase, PEG-SH can then be exchanged for the thiolated ligand of choice. The dynamics of place exchange of thiolate ligands on gold nanoparticle surfaces with thiols in solution have been studied extensively and used to prepare complex, mixed ligand shells as well as for complete ligand exchange.⁸⁹ In a ¹H NMR study of the exchange of PEG-SH and small carboxy- and amine-terminated alkanethiols on GNRs, Smith and co-workers found that the

exchange of PEG-SH for the small-molecule thiols was nearly complete but that the small-molecule thiols demonstrated very little exchange with other ligands.⁸⁰ They suggest that the PEG-SH molecules, because of their size and inter- and intramolecular interactions, form a less dense layer on the GNR surface. This leaves space for smaller thiolated ligands to bind to the GNR and form dense SAMs that displace PEG-SH, and GNR surfaces that are already functionalized with small thiolated ligands are not as readily accessible for ligand exchange on the gold surface.⁸⁰ Furthermore, the work of Smith et al. also demonstrates that the addition of new ligands does not always result in ligand exchange but that it is also possible for new ligands to “backfill” instead, leading to mixed-ligand systems.⁸⁰ Although mixed-ligand systems are well known to occur for SAMs of alkanethiolates on gold, it does highlight the importance of robust characterization methods when ligand-exchange methods are used in the synthesis of nanostructures from gold nanoparticles. Similarly, the complete removal of CTAB via ligand exchange is often difficult to achieve as a result of the relatively strong chemisorption of CTAB to the surface of GNRs. This is especially true for the aqueous PEG-SH functionalization of GNRs. In a recent study, small-angle neutron scattering measurements were used to show that after PEG-functionalization in aqueous solution the CTAB bilayer is still largely intact, and mass spectrometry confirmed the presence of CTAB.⁴⁴ Still, some ligand-exchange protocols have been shown to remove CTAB below the limits of detection of NMR and XPS.⁷⁹ Improved methods of characterization will better facilitate the quantification of residual CTAB, which will be necessary for developing better procedures for more thorough CTAB removal.

The anisotropy of gold nanorods allows for unique possibilities for ligand exchange. Compared to the sides of GNRs, the different crystal faces and the increased curvature on the ends of GNRs presents the opportunity to perform ligand exchange selectively on the ends. A number of studies have inferred selective functionalization of the ends of nanorods via

thiol and disulfide ligand exchange.⁹⁰ Factors contributing to the allegedly greater lability of the CTAB bilayer at the ends of gold nanorods compared to that on the sides that allow ligand exchange selectively at the ends may include differences in the packing CTAB at different crystal faces⁹¹ and the effects of increased curvature at the ends.^{75,92} Most of the evidence for end functionalization is indirect, verified mainly by TEM analysis showing the self-assembly of nanorods in an end-to-end configuration. This works because sample drying effects in non-end-to-end-functionalized GNRs produce a random mixture of GNRs with both end-to-end and side-by-side arrangements, with a preference for side-by-side resulting from a larger van der Waals interaction in the side-by-side configuration⁹³ that end-to-end ligand linking between GNRs sterically prevents.

III.D. Further Covalent Modification of Existing Ligand

Shells. Modification of the GNR surface can also be achieved through direct covalent attachment of ligands to existing ligands and polymers on the GNR surface. For example, many groups have functionalized GNRs with an azide-terminated ligand and used the copper-mediated Huisgen cycloaddition to covalently attach proteins and other biomolecules to the GNR using click chemistry. The first example of this was shown by Brust and co-workers, and they reported the covalent attachment of an acetylene-functionalized lipase to 14 nm gold nanospheres.⁹⁴ Our laboratory has extrapolated this technique to GNRs, wherein an acetylene-modified trypsin protein was covalently attached to azide-GNRs.⁹⁵ However, it was also noted in the study that trypsin immobilized on GNRs via this method did lose some biological activity when compared against free trypsin.

Furthermore, polymer initiators containing a sulfur derivative functional group can also be placed on the GNR for the purpose of altering the surface chemistry via polymer growth.^{96,97} The initiation of polymer growth on the surface of the GNR, reminiscent of the ATRP-mediated graft-from technique, yielded densely populated polymers that resulted in stable nanoparticle suspensions.^{97,98} For example, thermally responsive GNR complexes have been produced by grafting temperature-sensitive polymers such as poly(*N*-isopropylacrylamide) (PNIPAAm) or poly(methoxy-oligo(ethylene glycol) methacrylate) (PMOEGMA) from initiators covalently bound to the surface of GNRs (Figure 7).^{99,100} This technique was further extrapolated to GNRs by Wei et al., wherein they substituted the as-synthesized CTAB bilayer for a temperature-

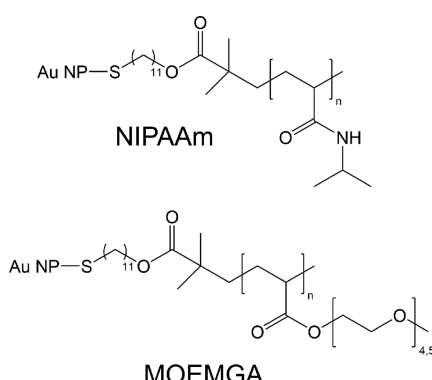


Figure 7. Chemical structures of poly(*N*-isopropylacrylamide) (NIPAAm) and poly(methoxy-*oligo*(ethylene glycol) methacrylate) (MOEGMA) bound to Au NPs via the initiator.

responsive polymer for the purposes of drug loading and delivery via the direct exposure of CTAB-coated GNRs to the disulfide polymer initiator.¹⁰¹

Additionally, polyelectrolytes used in layer-by-layer wrapping can also participate in modifying the surface chemistry by anchoring additional ligands to the surface of GNRs. For example, poly(acrylic acid) contains anionic carboxyl groups that can participate in 1-ethyl-3-(3-(dimethylamino)propyl)-carbodiimide (EDC)-mediated carbodiimide chemistry; we have shown the covalent attachment of biomolecules including biotin and the protein trypsin through this particular pathway.^{95,102} In the case of trypsin, however, the activity of the protein was severely hindered when attached to the GNR surface in this way. Compared to free trypsin, trypsin immobilized on a GNR via a carbodiimide retained only 13% of its activity, suggesting that potential active sites may be sterically hindered, or the conformation of the protein may be affected upon immobilization such that the enzymatic activity is limited.⁹⁵ For the purpose of attaching molecules with a specific active site or functional group, great care must be taken to ensure that the displayed orientation is desirable for the intended function because it was shown that different methods of attaching trypsin to GNRs have large effects on the protein's activity.^{95,102}

IV. CHARACTERIZATION AND MEASUREMENT CHALLENGES

As methods to modify the surface chemistry of gold nanoparticles become more advanced, it becomes increasingly important to understand the composition and morphology of the ligand shell because the surface chemistry of the nanoparticle determines how the nanoparticle will interact with its environment. The arrangement of ligands on the surface of gold nanorods or nanospheres in mixed monolayer systems can influence the nanoparticle wetting behavior,^{103,104} the interactions between the nanoparticle and cells,¹⁰⁵ and protein adsorption to nanoparticles,¹⁰⁶ in addition to playing a key role in applications such as self-assembly where site-specific functionalization is critical.^{75,102,107} Fully understanding the ligand shell involves addressing three main questions: (1) How thick is the ligand shell (e.g., monolayers vs multilayers)? (2) How many ligands are bound? (3) How are the ligands spatially distributed on the surface of the nanoparticle? These fundamental questions can be difficult to answer experimentally. However, once these questions can be answered for stable, static nanoparticles, they should be extended to the dynamic, changing nanoparticle surface chemistries found during the process of surface modification. The challenge of characterizing a dynamic surface on a nanoparticle will undoubtedly require the development of new characterization techniques and methodologies.

IV.A. How Thick Is the Ligand Shell?

microscopy is the preferred method for visualizing nanoparticle morphology, but the technique has limited utility when it comes to organic ligand capping agents. Transmission electron microscopy (TEM) can be quite useful in understanding core/shell nanoparticle structures and alloyed multimetallic particles. TEM is appropriate for core/shell analysis because the morphology of the hard shell will not be dramatically altered by drying the sample prior to imaging, and these materials have a higher Z contrast compared to that of organic capping agents.¹¹ Spectroscopic techniques that can be performed in a TEM such as electron energy loss spectroscopy (EELS) and

energy-dispersive X-ray spectroscopy (EDS) are routinely used to assess the spatial distribution of elements in core/shell or alloyed nanostructures.¹⁰⁸ These elemental analysis tools are critical to developing a complete picture of nanoparticle surface chemistry. For example, STEM-EDS imaging has been used to map out the distribution of trace levels of Ag on the surface of GNR in the quest to understand the role of Ag⁺ in the synthesis of GNRs.³¹ Trace element analysis demonstrates that the surface chemistry of GNRs is more complicated than an organic layer alone. The application of EELS and EDS becomes considerably more difficult if the shell is composed of organic ligands because of the low atomic numbers of the constituents.

Characterization of the dimensions of the solvated ligand shell is important. Dynamic light scattering (DLS) is a ubiquitous tool for the analysis of the hydrodynamic size distribution of colloidal particles. Comparing the size measured by DLS with the core nanoparticle size measured by TEM gives an approximate shell thickness. This is an approximate thickness because the hydrodynamic size encompasses the hydration shell that surrounds and moves with the particle as it diffuses through the bulk solvent. Most DLS instruments are best suited for and assume spherical nanoparticles, although it is possible to analyze anisotropic shapes such as rods by considering rotational diffusion coefficients.¹⁰⁹ A related technique known as nanoparticle tracking analysis (NTA) produces hydrodynamic size distributions by recording the Brownian motion of thousands of individual particles under optical dark-field conditions. In a study of citrate-capped GNRs, NTA has shown improved measurement precision over DLS where the relative standard deviation of the size distribution measurement was decreased from 31% using DLS to 11.4% using NTA.¹¹⁰ Under the conditions examined, the mode hydrodynamic diameter of citrate-stabilized GNRs measured by NTA closely matches the mean length measured by TEM, indicating that translational diffusion is effectively isotropic.

Small-angle scattering techniques such as small-angle X-ray scattering (SAXS) and small-angle neutron scattering (SANS) are alternative ensemble scattering measurement techniques that can be used to interrogate the thickness and structure of the ligand shell *in situ*. In SAXS, photons interact with the electron cloud; therefore, higher atomic numbers produce more scattering. In SANS, neutrons interact with nuclei, and the interaction depends on not only the number of protons but also the number of neutrons.^{111–113} Some light elements (e.g., deuterium) have scattering cross sections that are similar to those of heavy elements (e.g., lead). The most commonly examined element by SANS is hydrogen because the scattering from hydrogen is very distinct from that of its isotope, deuterium. Hydrogen is one of the few elements with a negative neutron scattering length density, meaning that neutrons scattered by hydrogen are 180° out of phase relative to those scattered by other elements as well as deuterium.^{111–113} These properties of hydrogen/deuterium scattering are very important for the technique of contrast matching, where varying the background solvent ratio of H₂O to D₂O varies the background scattering contrast and by matching the contrast of a constituent molecule in a mixture, the scattering from that component can be eliminated by background subtraction.

Although light-scattering techniques can give an estimate of overall thicknesses, SAXS and SANS provide further information about the organization and density of ligands on the surface.^{43,44} For example, Spalla et al. coupled SAXS and SANS to study the CTAB bilayer, and the SANS patterns

confirm that the thickness of the CTAB bilayer is on the order of 34 Å, corroborating conclusions drawn from TEM.⁹³ Beyond the thickness, this study emphasizes that the bilayer is compact and interdigitated because models of the SANS data that used a fully extended alkyl chain gave a thickness of 40 Å, and these models poorly represented the experimental data. Hammouda et al. performed a fascinating analysis using SANS of GNRs after ligand exchange by 5 kg/mol SH-PEG where the SANS patterns suggest that the CTAB bilayer is largely preserved even after ligand exchange.⁴⁴ Because PEG is commonly used to make nanomaterials biocompatible, this finding is particularly important considering that CTAB is toxic at micromolar concentrations to cells.

Electron microscopy can be applied to solvated nanoparticles as well via cryogenic electron microscopy. Rather than drying the nanoparticles on a grid, the liquid sample is vitrified by plunging it into liquid ethane and imaging it at cryogenic temperatures.¹¹⁴ This produces a solid sample compatible with the high-vacuum environment of the TEM where the nanoparticles are surrounded by an electron-transparent, amorphous matrix of vitreous water that preserves the solvated structure of the ligand shell for imaging. Examples of polyelectrolyte-wrapped gold nanorods imaged using cryo-TEM can be seen in Figure 8. The downside of cryo-TEM is that it is not a dynamic characterization technique capable of

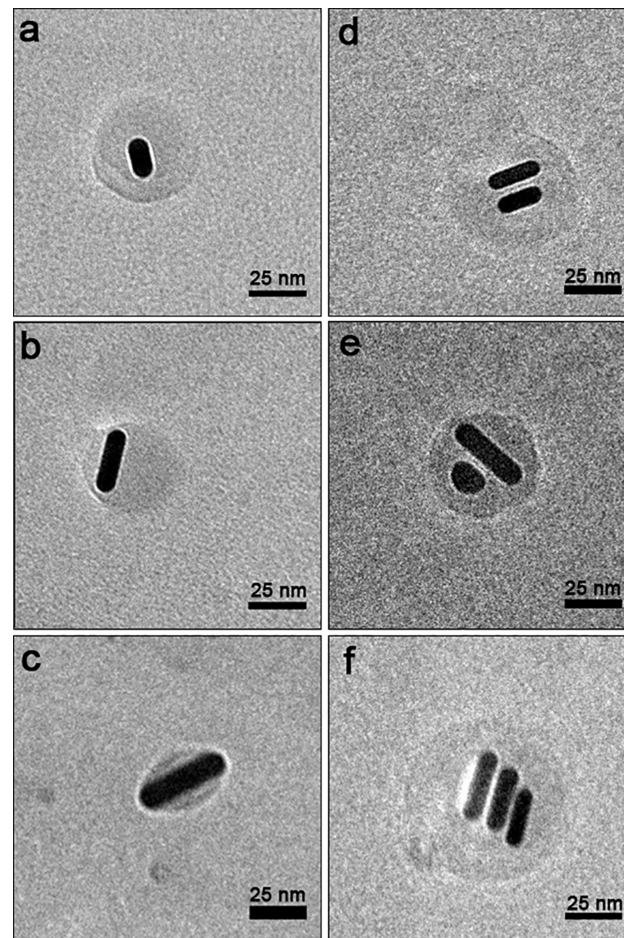


Figure 8. Cryo-TEM images of polyelectrolyte-wrapped gold nanorods illustrating the possible random structures that can be obtained in a single preparation including various (a–c) monomers, (d, e) dimers, and (f) trimers.

showing the coating processes in real time; however, the recent development of *in situ* liquid-cell TEM is a promising remedy to this drawback.¹¹⁵

IV.B. How Many Ligands Are There? The most sensitive approach to the quantification of surface ligands involves digesting the underlying gold nanoparticle core in *aqua regia* or a solution of potassium cyanide and then analyzing the digest to determine the concentration of ligands in solution using mass spectrometry with the inclusion of internal standards, although complementary results can be achieved with thermogravimetric analysis (TGA) or ¹H NMR.¹¹⁶ The ligand surface density is then estimated on the basis of the concentration of the nanoparticle solution, and the surface area of the nanoparticles is calculated on the basis of electron microscopy images. Various iterations of this approach involve tagging the ligands with a fluorophore or chromophore and using spectroscopic methods to quantify the ligands.¹¹⁷ Because of the low limits of detection (upwards of ppb) and high sensitivity of fluorescence measurements, this is a useful technique for nanoparticle analysis from a synthesis perspective in that it requires very little sample. Tagging can be particularly effective for nanoparticles modified with amines or carboxylate groups because of the varied chemistry available for further functionalization.¹¹⁸ However, it is critical that the degree of functionalization be known for accurate quantitation. Fluorescence measurements are frequently performed without dissolving the underlying nanoparticle, but this should be done with caution for plasmonic structures that can quench fluorescence.^{119,120}

Direct analysis of the nanoparticle surface to quantify ligands includes TGA and X-ray photoelectron spectroscopy (XPS). TGA measures the change in the mass of the nanoparticles as the sample is heated to cause decomposition and desorption of the ligands requiring sample sizes on the milligram scale (which is burdensome from a sample preparation standpoint) for accurate analysis.^{121,122} TGA alone is insufficient to determine the number of ligands per nanoparticle unless the mass of the underlying nanoparticle is well characterized.¹²³ If the mass is known accurately, then the measured change in mass due to the loss of the ligand shell and solvation shell can be used to determine the number of ligands and adsorbed solvent molecules per nanoparticle. Jin et al. used TGA to precisely determine the molecular formula for dried samples of gold nanocrystals capped with $-\text{SCH}_2\text{CH}_2\text{Ph}$.¹²⁴ The number of gold atoms making up the underlying nanoparticle (333 Au) was determined using electrospray ionization mass spectrometry, and TGA confirmed the number of ligands per nanoparticle to be 79. Ligand densities on spherical nanoparticles can also be quantified through XPS. XPS is highly surface-sensitive, probing only the top 5–10 nm of the sample, and can be used in both qualitative and quantitative capacities, making XPS useful for determining the efficacy of ligand exchange by quantifying the ligand densities on the surface.¹²⁵ In a qualitative capacity, XPS has a detection limit of 0.1% of the elemental composition, but for quantitative purposes, this level is 5%. Torelli et al. were able to quantify ligand densities on gold nanoparticles of varying diameters (1–18 nm) and capping ligands through experimental and computational analysis of XPS spectra by taking into account nanoparticle curvature.¹²⁶ On the basis of this method, the ligand-packing densities of $\text{HS}-(\text{CH}_2)_{11}-(\text{OCH}_2\text{CH}_2)_6\text{-COOH}$ and $\text{HS}-(\text{CH}_2)_{11}-(\text{OCH}_2\text{CH}_2)_6\text{-OH}$ were determined to be 3.9 ± 0.2 molecules nm^{-2} (less than the theoretical maximum of 4.6

molecules nm^{-2}), and the density did not change significantly with nanoparticle diameter. As shown by the preceding vignettes, the degree of accuracy with which ligand coverage can be determined is steadily improving, which is a critical component in the complete description of nanomaterials.

There are challenges inherent in any chosen method of ligand quantification. Any attempts to quantify the number of ligands on the surface of a nanoparticle must be preceded by careful cleaning to remove free ligand from the solution by methods such as centrifugation and dialysis. However, it is not possible to have a nanoparticle solution completely void of free ligand because the ligands on the surface of the nanoparticle are likely in dynamic equilibrium with ligands in solution. For example, CTAB-capped nanorods can survive only two rounds of centrifugation with dispersion in pure water to remove excess ligand; otherwise, with additional purification, the nanoparticles will aggregate because of the lack of CTAB in solution to maintain equilibrium on the surface with the accompanying surface charge stabilization of the suspension. This is true for electrostatically affixed capping agents and even thiolated ligands that are often thought of as covalently attached to the nanoparticle surface.^{89,127} The dynamic nature of nanoparticle surfaces has not thoroughly been considered in ligand quantification studies and warrants further discussion within the nanoparticle community because it plays a role in conventional quantification methods as well as new emerging methodologies (e.g., the detection of molecular vibrations unique to molecules adsorbed on GNRs measured by attenuated total reflectance infrared spectroscopy).¹²⁸

IV.C. Where Are Different Ligands? The question of ligand shell composition and morphology is key when discussing mixed self-assembled monolayer systems and site-specific nanoparticle functionalization. Many mixed ligand arrangements are possible, as depicted in Figure 9. Table 2

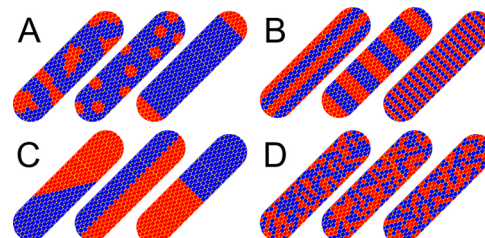


Figure 9. Depiction of possible mixed two-component thiolated ligand arrangements on gold nanorods, including (A) patchy, (B) striped, (C) Janus, and (D) random compositions.

details the most common tools for analyzing ligand shell morphology, along with the strengths and weaknesses associated with each. TEM imaging is relied upon heavily as the primary or even sole source of evidence for chemical anisotropy in self-assembly applications despite the indirect nature of the evidence, which highlights the need to expand and improve upon the tools available in this area.

Of the several techniques listed in Table 2, STM and NMR are the most promising methods to describe mixed monolayer ligand systems. Scanning tunneling microscopy (STM), previously employed to understand the phase separation of mixed-SAM systems on flat gold surfaces, has been extended to nanoparticles by Stellacci and co-workers.¹³⁰ On the curved surface of the particle, the length and ratio of thiolated ligands as well as the size of the underlying particle all contribute to

Table 2. Common Analytical Techniques Employed to Probe Mixed Ligand Shells on Nanoparticles

technique	knowledge gained	advantages	disadvantages	ref
Scanning Tunneling Microscopy (STM)	-pattern of and spacing between ligands -shell thickness	-nanoscale resolution on nanoparticles	-small sample size -high frequency, periodic noise, feedback artifacts	129–132
Nuclear Magnetic Resonance Spectroscopy (NMR)	-degrees of phase separation -domain organization -ligand quantification (after particle digestion)	-distinction among randomly mixed, Janus, and patchy ligand coatings by NOSEY technique -fairly ubiquitous instrument -many varieties of NMR	-small nanoparticles are most commonly studied (<10 nm) -requires highly concentrated samples	80, 123, 133–135
Transmission Electron Microscopy (TEM)	-visualize ligand arrangement/location through chemical staining or secondary nanoparticle tagging via conjugation chemistry	-visualize ligand shell, general arrangement, degree of patchiness, and number of patches	-small sample size -only for select ligands -often indirect evidence	136
Electron Spin Resonance (ESR)	-hydrophobicity using paramagnetic probes	-more sensitive than NMR due to shorter relaxation	-requires paramagnetic probe	137
Mass Spectrometry (MS)	-statistical quantification of ligand populations (after nanoparticle digestion) -degree of phase separation (matrix-assisted laser desorption ionization ion mobility mass spectrometry)	-compatible with most ligand mixtures - semiquantitative distinction among randomly mixed, Janus, and patchy ligand coatings	-ligand phase analysis requires a theoretical statistical model	138–140

differences in ligand arrangement and interdomain spacing of one ligand to the next ligand.^{129,141,142} The important roles of nanoparticle curvature and ligand stoichiometric ratio indicate that the phase separation of ligands is ordered and thermodynamically driven.¹²⁹ STM analysis as the sole source of evidence regarding ligand morphology is problematic because it has been demonstrated that scan parameters and feedback produce image artifacts.^{143,144} Therefore, STM is useful with complementary techniques such as NMR and FT-IR to ensure robust conclusions.

NMR is emerging as a major workhorse in the arena of ligand morphology because NMR spectra are rich with information about the chemical environment of the ligand.¹⁴⁵ Because of their size, nanoparticles tumble very slowly, resulting in lower signals and broader peaks for bound molecules than for free molecules, meaning that NMR of nanoparticle systems requires highly concentrated samples and longer collection times. However, the richness of the information that can be gained may outweigh these limitations. The NMR spectrum of ligand molecules on the surface of nanoparticles is influenced by the underlying nanoparticles and by coupling with neighboring ligands that provide a wealth of information regarding the local ligand environments on the surface of the particle. Pradhan et al. harnessed the coupling of ligands by performing nuclear Overhauser enhancement spectroscopy (NOESY), a 2D NMR technique, to differentiate between a randomly mixed monolayer and Janus nanoparticles coated with hexanethiolate and 2-(2-mercaptoethoxy)ethanol.¹³⁴ NOESY was further expanded by Stellacci and co-workers, who employed the technique to distinguish between nanoparticles with patchy domains as well as randomly mixed layers and Janus nanoparticles, both of which have distinct NOESY spectra and distinct profiles when the chemical shift is plotted with respect to the empirical chemical composition.¹³³ A similar pulse sequence named ROESY (rotating frame Overhauser effect spectroscopy) was employed by Fabris et al. to assess the

structure and integrity of peptides on a gold nanocluster.¹²³ Patchy nanoparticles have also been studied via paramagnetic relaxation enhancement where ligands are modified with Gd³⁺ ions that broaden the signals of molecules adjacent to the ion to the point where the signal disappears, providing direct evidence as to the structure of the mixed ligand surface.¹³⁵

Outside of mixed ligand systems, the sensitivity of NMR to the chemical environment provides insight into the packing and ordering of the ligand shell as well.¹⁴⁶ Areas of research where the interface between the nanoparticle surface and the surrounding environment are important, such as the protein coronas in biological systems, can also benefit from NMR. Determining the orientation of proteins adsorbed to nanoparticle surfaces is important for characterizing the protein corona, but this is difficult to measure. Lin et al. demonstrated that the orientation of protein α -synuclein adsorbed onto citrate and (16-mercaptophexadecyl)trimethylammonium bromide-capped nanospheres can be elucidated by heteronuclear single quantum coherence NMR spectroscopy to provide site-specific measurements of protein–nanoparticle binding due to the longer effective correlation times and weaker signals of amino acid residues closely associated with the nanoparticle surface.¹⁴⁷

The structure of the ligand shell of anisotropic nanoparticles such as gold nanorods has not been extensively studied. Fundamental questions regarding the structure of the CTAB bilayer could be confirmed if experimental requirements such as the high concentration of nanoparticles needed for NMR experiments can be met. For example, the CTAB bilayer is thought to be more loosely bound and labile on the ends of the nanorods versus the sides, creating distinct chemical environments for CTAB at the end of the rod versus the side of the rod, and also within the inner versus outer layers of the bilayer. By NMR, it could be possible to confirm site-specific functionalization such as ligand exchange by SH-PEG and

ultimately give unprecedented insight into the structure of the ligand shell.

A less common technique poised to greatly impact the characterization of nanoparticle surfaces, particularly the mapping of individual surface molecules, is super-resolution microscopy. Conventional light microscopy is limited in its spatial resolution by the diffraction of light to approximately 250 nm; however, various super-resolution techniques allow images to be taken with sub-100-nm spatial resolution.^{148,149} These techniques can be broadly classified into two categories of super-resolution: deterministic and stochastic. Deterministic methods exploit the nonlinear response of fluorophores to excitation to enhance resolution. Stochastic methods exploit a complex temporal behavior of molecular light sources arising from chemical complexity that enables neighboring fluorophores to be spatially resolved as a result of temporally separate light emissions, including super-resolution optical fluctuation imaging (SOFI) and all single-molecule localization methods (SMLM). The light emitted by a nanoscale object (i.e., a molecule) is from a point emitter that is below the diffraction limit of light, which causes the light to spread out in a distribution called a point spread function. The center of this distribution provides the location of the molecule, and an image of the structure to which the molecules are absorbed can be reconstructed from multiple locations of individual fluorophores. In SMLM, there are mainly two contributors to poor resolution and localization error in addition to error associated with the model used to fit the point spread function to determine its center.¹⁵⁰ The first is that most molecular dipole emitters are asymmetric and are attached to the surface in such a way as to still allow for rotational mobility about the point of attachment.¹⁵¹ Increased rotational mobility can cause increased degradation and distortion in super-resolution reconstructed images. The second is that not all objective lenses are created equal and some can induce point spread function aberrations that result in localization error.¹⁵⁰ Super-resolution microscopy has been successfully used to characterize molecular heterogeneity on the surface of thin films with both intentional, designed molecular patterns¹⁵² and random molecule placement.¹⁵³ Concerning the study of gold nanorods, super-resolution microscopy has thus far been successfully applied in studying how the localized surface plasmon is resonantly coupled to dipole emitters on their surface and its impact on their fluorescence emission and localization.^{154–156} Most super-resolution microscopy techniques are dependent on a probe molecule that fluoresces; however, methods are being developed that combine stimulated emission depletion microscopy with femtosecond stimulated Raman spectroscopy for label-free super-resolution microscopy.¹⁵⁷

V. FUTURE OUTLOOK

The anisotropy of gold nanorods presents both interesting synthesis possibilities and analytical challenges. Gold nanorods serve as a useful anisotropic model system to develop methods of precise control over anisotropic surface chemistries. For example, anisotropic ligand exchange has already been used to synthesize new nanostructures such as Wang et al.'s use of PEG-SH to block silica growth on the ends of nanorods, resulting in gold nanorods with a silica shell covering only the sides of the nanorod.⁷⁵ In the future, more direct measurements are necessary to fully understand the differences between the way that the ends and the sides are capped and to utilize those differences to build more complex nanomaterials. The development

and expansion of these methods to additional anisotropic materials has the potential to fill a synthetic nanoparticle surface chemistry toolbox analogous to that of synthetic organic chemistry and natural product synthesis. Such an ability to form complex nanostructures through site-specific surface chemistry will be important for potential future applications of gold nanorods in future technologies. Site-specific surface functionalization will enable the intentional design of increasingly complex structures of multiple anisotropic nanoparticles with a diverse array of surface chemistries with untold potential applications.

With these complex structures will come the need to characterize and confirm their synthesis that will drive the development of new and advanced characterization techniques, methodologies, and schemes. Of the techniques described here, NMR holds immediate and significant promise to yield useful information with regard to ligand arrangement and quantification on gold nanorods and should be applicable regardless of the core nanoparticle material. However, more advanced methods will also need to be developed that enable the dynamic observation of the nanoscale phenomena of coating and assembly in real time (e.g., *in situ* liquid–cell analytical transmission electron microscopy) as well as methods that characterize many individual nanoparticle surfaces to examine the surface variation between particles.

■ AUTHOR INFORMATION

Notes

The authors declare no competing financial interest.

Biographies



Nathan Burrows is a Wisconsin native and received his B.A. in chemistry and theatre from Concordia University, followed by his M.S. and Ph.D. in materials chemistry from the University of Minnesota—Twin Cities. He was a postdoctoral research assistant with Catherine J. Murphy at UIUC and is currently a postdoctoral scholar with Chris Keating at Pennsylvania State University.



Wayne Lin was born in Kaohsiung, Taiwan and was raised in New Zealand. He received his B.S. degree in chemistry from Rice University in 2012 and is currently pursuing a Ph.D. in chemistry from the University of Illinois at Urbana–Champaign under the tutelage of Professor Catherine J. Murphy.



Joshua G. Hinman is a native of Tremont, Illinois and received a B.S. degree in chemistry from Bradley University in Peoria, Illinois. He is currently a Ph.D. candidate at the University of Illinois at Urbana–Champaign studying with Professor Catherine J. Murphy.



Jordan M. Dennison is from Denver, Colorado and received her B.S. degree in chemistry from Colorado State University. She is currently a Ph.D. student at the University of Illinois at Urbana–Champaign studying with Professors Catherine J. Murphy and David Cahill.



Ariane M. Vartanian was born in northern California and received a B.A. in biochemistry from Swarthmore College and a Ph.D. in chemistry from the University of Illinois at Urbana–Champaign under the direction of Professors Catherine J. Murphy and Steven C. Zimmerman. She is currently an associate editor with *Nature Communications*.



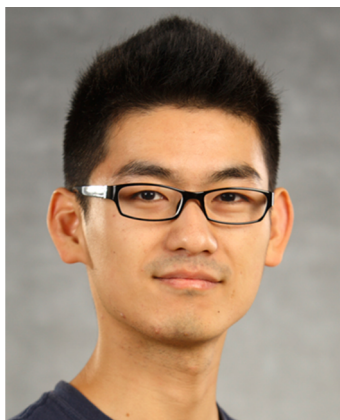
Nardine S. Abadeer was born in Alexandria, Egypt and grew up in Wisconsin. She received her B.Sc. in chemistry at the University of Minnesota—Twin Cities and her Ph.D. in materials chemistry at the University of Illinois at Urbana–Champaign. Nardine now works as an advanced scientist in the Science & Technology Development Program at Owens Corning.



Elissa M. Grzincic is a native of Michigan. She earned her B.S. degree in chemistry from the University of Michigan—Dearborn and her Ph.D. in chemistry from the University of Illinois at Urbana–Champaign with Professor Catherine J. Murphy in 2016. She is currently a postdoctoral fellow at the Molecular Foundry (Lawrence Berkeley National Laboratory) with Dr. Ronald N. Zuckermann of the Biological Nanostructures group.



Lisa M. Jacob is from Lexington, Massachusetts. She earned her B.A. degree in chemistry from Wellesley College. As a member of the Murphy group, she completed her M.S. degree in chemistry from the University of Illinois Urbana–Champaign and is currently working as a scientist at Corning Life Sciences.



Ji Li was born in Xi'an, China and graduated with a B.S. in chemistry from Tsinghua University. He now holds a master's degree in chemistry from the University of Illinois at Urbana–Champaign and is currently working towards a master's degree in statistics.



Catherine J. Murphy was born in New Jersey and grew up in suburban Chicago. She received two B.S. degrees (chemistry and biochemistry) from the University of Illinois at Urbana–Champaign in 1986, followed by a Ph.D. in chemistry from the University of Wisconsin—Madison in 1990. She was a postdoctoral fellow at the California Institute of Technology (1990–1993) before joining the faculty of the Department of Chemistry and Biochemistry at the University of South Carolina (1993–2009). In 2009, she returned to the University of Illinois at Urbana–Champaign as the Peter C. and Gretchen Miller Markunas Professor of Chemistry.

ACKNOWLEDGMENTS

We thank the National Science Foundation (CHE 1306596) for funding.

REFERENCES

- (1) Durr, N. J.; Larson, T.; Smith, D. K.; Korgel, B. A.; Sokolov, K.; Ben-Yakar, A. Two-Photon Luminescence Imaging of Cancer Cells Using Molecularly Targeted Gold Nanorods. *Nano Lett.* **2007**, *7* (4), 941–945.
- (2) Mayer, K. M.; Lee, S.; Liao, H.; Rostro, B. C.; Fuentes, A.; Scully, P. T.; Nehl, C. L.; Hafner, J. H. A Label-Free Immunoassay Based Upon Localized Surface Plasmon Resonance of Gold Nanorods. *ACS Nano* **2008**, *2* (4), 687–692.
- (3) von Maltzahn, G.; Park, J. H.; Agrawal, A.; Bandaru, N. K.; Das, S. K.; Sailor, M. J.; Bhatia, S. N. Computationally Guided Photothermal Tumor Therapy Using Long-Circulating Gold Nanorod Antennas. *Cancer Res.* **2009**, *69* (9), 3892–3900.
- (4) Min, Y.; Mao, C.; Xu, D.; Wang, J.; Liu, Y. Gold Nanorods for Platinum Based Prodrug Delivery. *Chem. Commun.* **2010**, *46* (44), 8424–3.
- (5) Li, A.; Zhang, P.; Chang, X.; Cai, W.; Wang, T.; Gong, J. Gold Nanorod@TiO₂ Yolk-Shell Nanostructures for Visible-Light-Driven Photocatalytic Oxidation of Benzyl Alcohol. *Small* **2015**, *11* (16), 1892–1899.
- (6) Han, X.; Liu, Y.; Yin, Y. Colorimetric Stress Memory Sensor Based on Disassembly of Gold Nanoparticle Chains. *Nano Lett.* **2014**, *14* (5), 2466–2470.
- (7) Lundén, H.; Liotta, A.; Chateau, D.; Lerouge, F.; Chaput, F.; Parola, S.; Brännlund, C.; Ghadyani, Z.; Kildemo, M.; Lindgren, M.; et al. Dispersion and Self-Orientation of Gold Nanoparticles in Sol–Gel Hybrid Silica – Optical Transmission Properties. *J. Mater. Chem. C* **2015**, *3* (5), 1026–1034.
- (8) Wu, X.; Liu, L.; Deng, Z.; Nian, L.; Zhang, W.; Hu, D.; Xie, Z.; Mo, Y.; Ma, Y. Efficiency Improvement in Polymer Light-Emitting Diodes by “Far-Field” Effect of Gold Nanoparticles. *Part. Part. Syst. Charact.* **2015**, *32* (6), 686–692.
- (9) Mubeen, S.; Lee, J.; Lee, W.-R.; Singh, N.; Stucky, G. D.; Moskovits, M. On the Plasmonic Photovoltaic. *ACS Nano* **2014**, *8* (6), 6066–6073.
- (10) Link, S.; Mohamed, M. B.; El-Sayed, M. A. Simulation of the Optical Absorption Spectra of Gold Nanorods as a Function of Their Aspect Ratio and the Effect of the Medium Dielectric Constant. *J. Phys. Chem. B* **1999**, *103* (16), 3073–3077.
- (11) Abadeer, N. S.; Brennan, M. R.; Wilson, W. L.; Murphy, C. J. Distance and Plasmon Wavelength Dependent Fluorescence of Molecules Bound to Silica-Coated Gold Nanorods. *ACS Nano* **2014**, *8* (8), 8392–8406.
- (12) Sivapalan, S. T.; DeVetter, B. M.; Yang, T. K.; van Dijk, T.; Schulmerich, M. V.; Carney, P. S.; Bhargava, R.; Murphy, C. J. Off-Resonance Surface-Enhanced Raman Spectroscopy From Gold Nanorod Suspensions as a Function of Aspect Ratio: Not What We Thought. *ACS Nano* **2013**, *7* (3), 2099–2105.
- (13) Sivapalan, S. T.; Vella, J. H.; Yang, T. K.; Dalton, M. J.; Swiger, R. N.; Haley, J. E.; Cooper, T. M.; Urbas, A. M.; Tan, L.-S.; Murphy, C. J. Plasmonic Enhancement of the Two Photon Absorption Cross Section of an Organic Chromophore Using Polyelectrolyte-Coated Gold Nanorods. *Langmuir* **2012**, *28* (24), 9147–9154.
- (14) Burrows, N. D.; Vartanian, A. M.; Abadeer, N. S.; Grzincic, E. M.; Jacob, L. M.; Lin, W.; Li, J.; Dennison, J. M.; Hinman, J. G.; Murphy, C. J. Anisotropic Nanoparticles and Anisotropic Surface Chemistry. *J. Phys. Chem. Lett.* **2016**, *7* (4), 632–641.
- (15) Yang, J. A.; Phan, H. T.; Vaidya, S.; Murphy, C. J. Nanovacuums: Nanoparticle Uptake and Differential Cellular Migration on a Carpet of Nanoparticles. *Nano Lett.* **2013**, *13* (5), 2295–2302.
- (16) Grzincic, E. M.; Yang, J. A.; Drnevich, J.; Falagan-Lotsch, P.; Murphy, C. J. Global Transcriptomic Analysis of Model Human Cell

- Lines Exposed to Surface-Modified Gold Nanoparticles: the Effect of Surface Chemistry. *Nanoscale* **2015**, *7* (4), 1349–1362.
- (17) Alkilany, A. M.; Murphy, C. J. Toxicity and Cellular Uptake of Gold Nanoparticles: What We Have Learned So Far? *J. Nanopart. Res.* **2010**, *12* (7), 2313–2333.
- (18) Wu, B.; Liu, D.; Mubeen, S.; Chuong, T. T.; Moskovits, M.; Stucky, G. D. Anisotropic Growth of TiO₂ onto Gold Nanorods for Plasmon-Enhanced Hydrogen Production From Water Reduction. *J. Am. Chem. Soc.* **2016**, *138* (4), 1114–1117.
- (19) Murphy, C. J.; Thompson, L. B.; Chernak, D. J.; Yang, J. A.; Sivapalan, S. T.; Boulos, S. P.; Huang, J.; Alkilany, A. M.; Sisco, P. N. Gold Nanorod Crystal Growth: From Seed-Mediated Synthesis to Nanoscale Sculpting. *Curr. Opin. Colloid Interface Sci.* **2011**, *16* (2), 128–134.
- (20) Jana, N. R.; Gearheart, L.; Murphy, C. J. Wet Chemical Synthesis of High Aspect Ratio Cylindrical Gold Nanorods. *J. Phys. Chem. B* **2001**, *105* (19), 4065–4067.
- (21) Jana, N. R.; Gearheart, L.; Murphy, C. J. Seed-Mediated Growth Approach for Shape-Controlled Synthesis of Spheroidal and Rod-Like Gold Nanoparticles Using a Surfactant Template. *Adv. Mater.* **2001**, *13* (18), 1389.
- (22) Nikoobakht, B.; El-Sayed, M. A. Preparation and Growth Mechanism of Gold Nanorods (NRs) Using Seed-Mediated Growth Method. *Chem. Mater.* **2003**, *15* (10), 1957–1962.
- (23) Scarabelli, L.; Grzelczak, M.; Liz-Marzán, L. M. Tuning Gold Nanorod Synthesis Through Prereduction with Salicylic Acid. *Chem. Mater.* **2013**, *25* (21), 4232–4238.
- (24) Ye, X.; Zheng, C.; Chen, J.; Gao, Y.; Murray, C. B. Using Binary Surfactant Mixtures to Simultaneously Improve the Dimensional Tunability and Monodispersity in the Seeded Growth of Gold Nanorods. *Nano Lett.* **2013**, *13* (2), 765–771.
- (25) Vigderman, L.; Zubarev, E. R. High-Yield Synthesis of Gold Nanorods with Longitudinal SPR Peak Greater Than 1200 nm Using Hydroquinone as a Reducing Agent. *Chem. Mater.* **2013**, *25* (8), 1450–1457.
- (26) Altansukh, B.; Yao, J.; Wang, D. Synthesis and Characterization of Gold Nanorods by a Seeding Growth Method. *J. Nanosci. Nanotechnol.* **2009**, *9* (2), 1300–1303.
- (27) Busbee, B. D.; Obare, S. O.; Murphy, C. J. An Improved Synthesis of High-Aspect-Ratio Gold Nanorods. *Adv. Mater.* **2003**, *15* (5), 414–416.
- (28) Grzelczak, M.; Pérez-Juste, J.; Mulvaney, P.; Liz-Marzán, L. M. Shape Control in Gold Nanoparticle Synthesis. *Chem. Soc. Rev.* **2008**, *37* (9), 1783–10.
- (29) Orendorff, C. J.; Murphy, C. J. Quantitation of Metal Content in the Silver-Assisted Growth of Gold Nanorods. *J. Phys. Chem. B* **2006**, *110* (9), 3990–3994.
- (30) Grzelczak, M.; Sánchez-Iglesias, A.; Rodríguez-González, B.; Alvarez-Puebla, R.; Pérez-Juste, J.; Liz-Marzán, L. M. Influence of Iodide Ions on the Growth of Gold Nanorods: Tuning Tip Curvature and Surface Plasmon Resonance. *Adv. Funct. Mater.* **2008**, *18* (23), 3780–3786.
- (31) Jackson, S. R.; McBride, J. R.; Rosenthal, S. J.; Wright, D. W. Where's the Silver? Imaging Trace Silver Coverage on the Surface of Gold Nanorods. *J. Am. Chem. Soc.* **2014**, *136* (14), 5261–5263.
- (32) Giannici, F.; Placido, T.; Curri, M. L.; Striccoli, M.; Agostiano, A.; Comparelli, R. The Fate of Silver Ions in the Photochemical Synthesis of Gold Nanorods: an Extended X-Ray Absorption Fine Structure Analysis. *Dalton Trans.* **2009**, 10367–10368.
- (33) Hubert, F.; Testard, F.; Spalla, O. Cetyltrimethylammonium Bromide Silver Bromide Complex as the Capping Agent of Gold Nanorods. *Langmuir* **2008**, *24* (17), 9219–9222.
- (34) Liao, H.; Hafner, J. H. Gold Nanorod Bioconjugates. *Chem. Mater.* **2005**, *17* (18), 4636–4641.
- (35) Zhang, Q.; Jing, H.; Li, G. G.; Lin, Y.; Bloni, D. A.; Wang, H. Intertwining Roles of Silver Ions, Surfactants, and Reducing Agents in Gold Nanorod Overgrowth: Pathway Switch Between Silver Underpotential Deposition and Gold-Silver Codeposition. *Chem. Mater.* **2016**, *28* (8), 2728–2741.
- (36) Niidome, Y.; Nakamura, Y.; Honda, K.; Akiyama, Y.; Nishioka, K.; Kawasaki, H.; Nakashima, N. Characterization of Silver Ions Adsorbed on Gold Nanorods: Surface Analysis by Using Surface-Assisted Laser Desorption/Ionization Time-of-Flight Mass Spectrometry. *Chem. Commun.* **2009**, 1754–1756.
- (37) Ye, X.; Gao, Y.; Chen, J.; Reifsnyder, D. C.; Zheng, C.; Murray, C. B. Seeded Growth of Monodisperse Gold Nanorods Using Bromide-Free Surfactant Mixtures. *Nano Lett.* **2013**, *13* (5), 2163–2171.
- (38) Sau, T. K.; Murphy, C. J. Role of Ions in the Colloidal Synthesis of Gold Nanowires. *Philos. Mag.* **2007**, *87* (14–15), 2143–2158.
- (39) Garg, N.; Scholl, C.; Mohanty, A.; Jin, R. The Role of Bromide Ions in Seeding Growth of Au Nanorods. *Langmuir* **2010**, *26* (12), 10271–10276.
- (40) Lohse, S. E.; Burrows, N. D.; Scarabelli, L.; Liz-Marzán, L. M.; Murphy, C. J. Anisotropic Noble Metal Nanocrystal Growth: the Role of Halides. *Chem. Mater.* **2014**, *26* (1), 34–43.
- (41) Gao, J.; Bender, C. M.; Murphy, C. J. Dependence of the Gold Nanorod Aspect Ratio on the Nature of the Directing Surfactant in Aqueous Solution. *Langmuir* **2003**, *19* (21), 9065–9070.
- (42) Nikoobakht, B.; El-Sayed, M. A. Evidence for Bilayer Assembly of Cationic Surfactants on the Surface of Gold Nanorods. *Langmuir* **2001**, *17* (20), 6368–6374.
- (43) Gómez-Graña, S.; Hubert, F.; Testard, F.; Guerrero-Martínez, A.; Grillo, I.; Liz-Marzán, L. M.; Spalla, O. Surfactant (Bi)Layers on Gold Nanorods. *Langmuir* **2012**, *28* (2), 1453–1459.
- (44) Hore, M. J. A.; Ye, X.; Ford, J.; Gao, Y.; Fei, J.; Wu, Q.; Rowan, S. J.; Composto, R. J.; Murray, C. B.; Hammouda, B. Probing the Structure, Composition, and Spatial Distribution of Ligands on Gold Nanorods. *Nano Lett.* **2015**, *15* (9), 5730–5738.
- (45) Schmidt, T.; Schütz, G. J.; Baumgartner, W.; Gruber, H. J.; Schindler, H. Imaging of Single Molecule Diffusion. *Proc. Natl. Acad. Sci. U. S. A.* **1996**, *93* (7), 2926–2929.
- (46) Schunack, M.; Linderoth, T. R.; Rosei, F.; Lægsgaard, E.; Stensgaard, I.; Besenbacher, F. Long Jumps in the Surface Diffusion of Large Molecules. *Phys. Rev. Lett.* **2002**, *88* (15), 156102–156104.
- (47) Soliman, M. G.; Pelaz, B.; Parak, W. J.; del Pino, P. Phase Transfer and Polymer Coating Methods Toward Improving the Stability of Metallic Nanoparticles for Biological Applications. *Chem. Mater.* **2015**, *27* (3), 990–997.
- (48) Alkilany, A. M.; Yaseen, A. I. B.; Park, J.; Eller, J. R.; Murphy, C. J. Facile Phase Transfer of Gold Nanoparticles From Aqueous Solution to Organic Solvents with Thiolated Poly(Ethylene Glycol). *RSC Adv.* **2014**, *4* (95), 52676–52679.
- (49) Lista, M.; Liu, D. Z.; Mulvaney, P. Phase Transfer of Noble Metal Nanoparticles to Organic Solvents. *Langmuir* **2014**, *30* (8), 1932–1938.
- (50) Gole, A.; Murphy, C. J. Polyelectrolyte-Coated Gold Nanorods: Synthesis, Characterization and Immobilization. *Chem. Mater.* **2005**, *17* (6), 1325–1330.
- (51) Hauck, T. S.; Ghazani, A. A.; Chan, W. C. W. Assessing the Effect of Surface Chemistry on Gold Nanorod Uptake, Toxicity, and Gene Expression in Mammalian Cells. *Small* **2008**, *4* (1), 153–159.
- (52) Alkilany, A. M.; Nagaria, P. K.; Hexel, C. R.; Shaw, T. J.; Murphy, C. J.; Wyatt, M. D. Cellular Uptake and Cytotoxicity of Gold Nanorods: Molecular Origin of Cytotoxicity and Surface Effects. *Small* **2009**, *5* (6), 701–708.
- (53) Sisco, P. N.; Wilson, C. G.; Chernak, D.; Clark, J. C.; Grzincic, E. M.; Ako-Asare, K.; Goldsmith, E. C.; Murphy, C. J. Adsorption of Cellular Proteins to Polyelectrolyte-Functionalized Gold Nanorods: a Mechanism for Nanoparticle Regulation of Cell Phenotype? *PLoS One* **2014**, *9* (2), e86670–e86678.
- (54) Ni, W.; Yang, Z.; Chen, H.; Li, L.; Wang, J. Coupling Between Molecular and Plasmonic Resonances in Freestanding Dye-Gold Nanorod Hybrid Nanostructures. *J. Am. Chem. Soc.* **2008**, *130* (21), 6692.
- (55) Gandra, N.; Portz, C.; Tian, L.; Tang, R.; Xu, B.; Achilefu, S.; Singamaneni, S. Probing Distance-Dependent Plasmon-Enhanced

- Near-Infrared Fluorescence Using Polyelectrolyte Multilayers as Dielectric Spacers. *Angew. Chem., Int. Ed.* **2014**, *53* (3), 866–870.
- (56) DeVetter, B. M.; Sivapalan, S. T.; Patel, D. D.; Schulmerich, M. V.; Murphy, C. J.; Bhargava, R. Observation of Molecular Diffusion in Polyelectrolyte-Wrapped SERS Nanoprobes. *Langmuir* **2014**, *30* (29), 8931–8937.
- (57) Huang, J.; Jackson, K. S.; Murphy, C. J. Polyelectrolyte Wrapping Layers Control Rates of Photothermal Molecular Release From Gold Nanorods. *Nano Lett.* **2012**, *12* (6), 2982–2987.
- (58) Park, H.; Lee, S.; Chen, L.; Lee, E. K.; Shin, S. Y.; Lee, Y. H.; Son, S. W.; Oh, C. H.; Song, J. M.; Kang, S. H.; et al. SERS Imaging of HER2-Overexpressed MCF7 Cells Using Antibody-Conjugated Gold Nanorods. *Phys. Chem. Chem. Phys.* **2009**, *11* (34), 7444–7449.
- (59) Kirui, D. K.; Krishnan, S.; Strickland, A. D.; Batt, C. A. PAA-Derived Gold Nanorods for Cellular Targeting and Photothermal Therapy. *Macromol. Biosci.* **2011**, *11* (6), 779–788.
- (60) Agarwal, A.; Huang, S. W.; O'Donnell, M.; Day, K. C.; Day, M.; Kotov, N.; Ashkenazi, S. Targeted Gold Nanorod Contrast Agent for Prostate Cancer Detection by Photoacoustic Imaging. *J. Appl. Phys.* **2007**, *102* (6), 064701.
- (61) Liz-Marzán, L. M.; Giersig, M.; Mulvaney, P. Synthesis of Nanosized Gold-Silica Core-Shell Particles. *Langmuir* **1996**, *12* (18), 4329–4335.
- (62) Gorelikov, I.; Matsuura, N. Single-Step Coating of Mesoporous Silica on Cetyltrimethyl Ammonium Bromide-Capped Nanoparticles. *Nano Lett.* **2008**, *8* (1), 369–373.
- (63) Liu, J.; Detrembleur, C.; De Pauw-Gillet, M.-C.; Mornet, S.; Jerome, C.; Duguet, E. Gold Nanorods Coated with Mesoporous Silica Shell as Drug Delivery System for Remote Near Infrared Light-Activated Release and Potential Phototherapy. *Small* **2015**, *11* (19), 2323–2332.
- (64) Wu, W.-C.; Tracy, J. B. Large-Scale Silica Overcoating of Gold Nanorods with Tunable Shell Thicknesses. *Chem. Mater.* **2015**, *27* (8), 2888–2894.
- (65) Roca, M.; Haes, A. J. Silica–Void–Gold Nanoparticles: Temporally Stable Surface-Enhanced Raman Scattering Substrates. *J. Am. Chem. Soc.* **2008**, *130* (43), 14273–14279.
- (66) Zhao, D.; Feng, J.; Huo, Q.; Melosh, N.; Fredrickson, G. H.; Chmelka, B. F.; Stucky, G. D. Triblock Copolymer Syntheses of Mesoporous Silica with Periodic 50 to 300 Angstrom Pores. *Science* **1998**, *279* (5350), 548–552.
- (67) Stöber, W.; Fink, A.; Bohn, E. Controlled Growth of Monodisperse Silica Spheres in the Micron Size Range. *J. Colloid Interface Sci.* **1968**, *26* (1), 62–69.
- (68) Brinker, C. J.; Scherer, G. W. *Sol Gel Science*; Academic Press: San Diego, CA, 1990.
- (69) Lin, Y.-S.; Abadeer, N.; Hurley, K. R.; Haynes, C. L. Ultrastable, Redispersible, Small, and Highly Organomodified Mesoporous Silica Nanotherapeutics. *J. Am. Chem. Soc.* **2011**, *133* (50), 20444–20457.
- (70) Nooney, R. I.; Thirunavukkarasu, D.; Chen, Y.; Josephs, R.; Ostafin, A. E. Self-Assembly of Mesoporous Nanoscale Silica/Gold Composites. *Langmuir* **2003**, *19* (18), 7628–7637.
- (71) Goyal, P. S.; Dasannacharya, B. A.; Kelkar, V. K.; Manohar, C.; Rao, K. S.; Valaulikar, B. S. Shapes and Sizes of Micelles in CTAB Solutions. *Physica B* **1991**, *174* (1–4), 196–199.
- (72) Cifuentes, A.; Bernal, J. L.; DiezMasa, J. C. Determination of Critical Micelle Concentration Values Using Capillary Electrophoresis Instrumentation. *Anal. Chem.* **1997**, *69* (20), 4271–4274.
- (73) Cong, H.; Toftegaard, R.; Arnbjerg, J.; Ogilby, P. R. Silica-Coated Gold Nanorods with a Gold Overcoat: Controlling Optical Properties by Controlling the Dimensions of a Gold–Silica–Gold Layered Nanoparticle. *Langmuir* **2010**, *26* (6), 4188–4195.
- (74) Liu, W.; Zhu, Z.; Deng, K.; Li, Z.; Zhou, Y.; Qiu, H.; Gao, Y.; Che, S.; Tang, Z. Gold Nanorod@Chiral Mesoporous Silica Core–Shell Nanoparticles with Unique Optical Properties. *J. Am. Chem. Soc.* **2013**, *135* (26), 9659–9664.
- (75) Wang, F.; Cheng, S.; Bao, Z.; Wang, J. Anisotropic Overgrowth of Metal Heterostructures Induced by a Site-Selective Silica Coating. *Angew. Chem., Int. Ed.* **2013**, *52* (39), 10344–10348.
- (76) Sanz-Ortiz, M. N.; Sentosun, K.; Bals, S.; Liz-Marzán, L. M. Templated Growth of Surface Enhanced Raman Scattering-Active Branched Gold Nanoparticles Within Radial Mesoporous Silica Shells. *ACS Nano* **2015**, *9* (10), 10489–10497.
- (77) Tang, H.; Shen, S.; Guo, J.; Chang, B.; Jiang, X.; Yang, W. Gold Nanorods@mSiO₂ with a Smart Polymer Shell Responsive to Heat/Near-Infrared Light for Chemo-Photothermal Therapy. *J. Mater. Chem.* **2012**, *22* (31), 16095–16103.
- (78) Shen, S.; Tang, H.; Zhang, X.; Ren, J.; Pang, Z.; Wang, D.; Gao, H.; Qian, Y.; Jiang, X.; Yang, W. Targeting Mesoporous Silica-Encapsulated Gold Nanorods for Chemo-Photothermal Therapy with Near-Infrared Radiation. *Biomaterials* **2013**, *34* (12), 3150–3158.
- (79) Indrasekara, A. S. D. S.; Wadams, R. C.; Fabris, L. Ligand Exchange on Gold Nanorods: Going Back to the Future. *Part. Part. Syst. Charact.* **2014**, *31* (8), 819–838.
- (80) Smith, A. M.; Marbella, L. E.; Johnston, K. A.; Hartmann, M. J.; Crawford, S. E.; Kozycz, L. M.; Seferos, D. S.; Millstone, J. E. Quantitative Analysis of Thiolated Ligand Exchange on Gold Nanoparticles Monitored by ¹H NMR Spectroscopy. *Anal. Chem.* **2015**, *87* (5), 2771–2778.
- (81) Oyerokun, F. T.; Vaia, R. A.; Maguire, J. F.; Farmer, B. L. Role of Solvent Selectivity in the Equilibrium Surface Composition of Monolayers Formed From a Solution Containing Mixtures of Organic Thiols. *Langmuir* **2010**, *26* (14), 11991–11997.
- (82) Dubois, L. H.; Nuzzo, R. G. Synthesis, Structure, and Properties of Model Organic Surfaces. *Annu. Rev. Phys. Chem.* **1992**, *43*, 437.
- (83) Love, J. C.; Estroff, L. A.; Kriebel, J. K.; Nuzzo, R. G.; Whitesides, G. M. Self-Assembled Monolayers of Thiolates on Metals as a Form of Nanotechnology. *Chem. Rev.* **2005**, *105* (4), 1103–1170.
- (84) Hinterwirth, H.; Kappel, S.; Waitz, T.; Prohaska, T.; Lindner, W.; Lämmerhofer, M. Quantifying Thiol Ligand Density of Self-Assembled Monolayers on Gold Nanoparticles by Inductively Coupled Plasma–Mass Spectrometry. *ACS Nano* **2013**, *7* (2), 1129–1136.
- (85) Djebaili, T.; Richardi, J.; Abel, S.; Marchi, M. Atomistic Simulations of Self-Assembled Monolayers on Octahedral and Cubic Gold Nanocrystals. *J. Phys. Chem. C* **2015**, *119* (36), 21146–21154.
- (86) Biju, V. Chemical Modifications and Bioconjugate Reactions of Nanomaterials for Sensing, Imaging, Drug Delivery and Therapy. *Chem. Soc. Rev.* **2014**, *43* (3), 744.
- (87) Wijaya, A.; Hamad-Schifferli, K. Ligand Customization and DNA Functionalization of Gold Nanorods via Round-Trip Phase Transfer Ligand Exchange. *Langmuir* **2008**, *24* (18), 9966–9969.
- (88) Liu, M.; Law, W.-C.; Kopwitthaya, A.; Liu, X.; Swihart, M. T.; Prasad, P. N. Exploring the Amphiphilicity of PEGylated Gold Nanorods: Mechanical Phase Transfer and Self-Assembly. *Chem. Commun.* **2013**, *49* (81), 9350–9353.
- (89) Hostetler, M. J.; Templeton, A. C.; Murray, R. W. Dynamics of Place-Exchange Reactions on Monolayer-Protected Gold Cluster Molecules. *Langmuir* **1999**, *15* (11), 3782–3789.
- (90) Nie, Z.; Fava, D.; Kumacheva, E.; Zou, S.; Walker, G. C.; Rubinstein, M. Self-Assembly of Metal–Polymer Analogues of Amphiphilic Triblock Copolymers. *Nat. Mater.* **2007**, *6* (8), 609–614.
- (91) Meena, S. K.; Sulpizi, M. Understanding the Microscopic Origin of Gold Nanoparticle Anisotropic Growth From Molecular Dynamics Simulations. *Langmuir* **2013**, *29* (48), 14954–14961.
- (92) Kou, X.; Sun, Z.; Yang, Z.; Chen, H.; Wang, J. Curvature-Directed Assembly of Gold Nanocubes, Nanobranches, and Nanospheres. *Langmuir* **2009**, *25* (3), 1692–1698.
- (93) Sau, T. K.; Murphy, C. J. Self-Assembly Patterns Formed Upon Solvent Evaporation of Aqueous Cetyltrimethylammonium Bromide-Coated Gold Nanoparticles of Various Shapes. *Langmuir* **2005**, *21* (7), 2923–2929.
- (94) Brennan, J. L.; Hatzakis, N. S.; Tshikhudo, T. R.; Dirvianskyte, N.; Razumas, V.; Patkar, S.; Vind, J.; Svendsen, A.; Nolte, R. J. M.; Rowan, A. E.; et al. Bionanoconjugation via Click Chemistry: the Creation of Functional Hybrids of Lipases and Gold Nanoparticles. *Bioconjugate Chem.* **2006**, *17* (6), 1373–1375.

- (95) Gole, A.; Murphy, C. J. Azide-Derivatized Gold Nanorods: Functional Materials for “Click” Chemistry. *Langmuir* **2008**, *24* (1), 266–272.
- (96) Watson, K. J.; Zhu, J.; Nguyen, S. T.; Mirkin, C. A. Hybrid Nanoparticles with Block Copolymer Shell Structures. *J. Am. Chem. Soc.* **1999**, *121* (2), 462–463.
- (97) Jordan, R.; West, N.; Ulman, A.; Chou, Y. M.; Nuyken, O. Nanocomposites by Surface-Initiated Living Cationic Polymerization of 2-Oxazolines on Functionalized Gold Nanoparticles. *Macromolecules* **2001**, *34* (6), 1606–1611.
- (98) Mandal, T. K.; Fleming, M. S.; Walt, D. R. Preparation of Polymer Coated Gold Nanoparticles by Surface-Confining Living Radical Polymerization at Ambient Temperature. *Nano Lett.* **2002**, *2* (1), 3–7.
- (99) Kim, D. J.; Kang, S. M.; Kong, B.; Kim, W. J.; Paik, H. J.; Choi, H.; Choi, I. S. Formation of Thermoresponsive Gold Nanoparticle/PNIPAAm Hybrids by Surface-Initiated, Atom Transfer Radical Polymerization in Aqueous Media. *Macromol. Chem. Phys.* **2005**, *206* (19), 1941–1946.
- (100) Li, D.; Cui, Y.; Wang, K.; He, Q.; Yan, X.; Li, J. Thermosensitive Nanostructures Comprising Gold Nanoparticles Grafted with Block Copolymers. *Adv. Funct. Mater.* **2007**, *17* (16), 3134–3140.
- (101) Wei, Q.; Ji, J.; Shen, J. Synthesis of Near-Infrared Responsive Gold Nanorod/PNIPAAm Core/Shell Nanohybrids via Surface Initiated ATRP for Smart Drug Delivery. *Macromol. Rapid Commun.* **2008**, *29* (8), 645–650.
- (102) Gole, A.; Murphy, C. J. Biotin–Streptavidin-Induced Aggregation of Gold Nanorods: Tuning Rod–Rod Orientation. *Langmuir* **2005**, *21* (23), 10756–10762.
- (103) Liu, S.-J.; Li, Y.-J.; Wang, Y.-M.; Liu, X.; Yeung, E. S. Two-Dimensional Self-Assembly of Hydrophobic Nanoparticles at Oil/Water Interfaces via Nanoscale Phase Separation of Mixed Ligands. *J. Colloid Interface Sci.* **2013**, *407*, 243–249.
- (104) Centrone, A.; Penzo, E.; Sharma, M.; Myerson, J. W.; Jackson, A. M.; Marzari, N.; Stellacci, F. The Role of Nanostructure in the Wetting Behavior of Mixed-Monolayer-Protected Metal Nanoparticles. *Proc. Natl. Acad. Sci. U. S. A.* **2008**, *105* (29), 9886–9891.
- (105) Verma, A.; Stellacci, F. Effect of Surface Properties on Nanoparticle-Cell Interactions. *Small* **2010**, *6* (1), 12–21.
- (106) Huang, R.; Carney, R. R.; Ikuma, K.; Stellacci, F.; Lau, B. L. T. Effects of Surface Compositional and Structural Heterogeneity on Nanoparticle-Protein Interactions: Different Protein Configurations. *ACS Nano* **2014**, *8* (6), 5402–5412.
- (107) Chen, T.; Du, C.; Tan, L. H.; Shen, Z.; Chen, H. Site-Selective Localization of Analytes on Gold Nanorod Surface for Investigating Field Enhancement Distribution in Surface-Enhanced Raman Scattering. *Nanoscale* **2011**, *3* (4), 1575–1581.
- (108) Chaudhuri, R. G.; Paria, S. Core/Shell Nanoparticles: Classes, Properties, Synthesis Mechanisms, Characterization, and Applications. *Chem. Rev.* **2012**, *112* (4), 2373–2433.
- (109) Rodríguez-Fernández, J.; Pérez-Juste, J.; Liz-Marzáñ, L. M.; Lang, P. R. Dynamic Light Scattering of Short Au Rods with Low Aspect Ratios. *J. Phys. Chem. C* **2007**, *111* (13), 5020–5025.
- (110) Mehtala, J. G.; Wei, A. Nanometric Resolution in the Hydrodynamic Size Analysis of Ligand-Stabilized Gold Nanorods. *Langmuir* **2014**, *30* (46), 13737–13743.
- (111) Hammouda, B.; Krueger, S.; Glinka, C. J. Small-Angle Neutron-Scattering at the National-Institute-of-Standards-and-Technology. *J. Res. Natl. Inst. Stand. Technol.* **1993**, *98* (1), 31–46.
- (112) Chen, S. H. Small-Angle Neutron-Scattering Studies of the Structure and Interaction in Micellar and Microemulsion Systems. *Annu. Rev. Phys. Chem.* **1986**, *37* (1), 351–399.
- (113) Svergun, D. I.; Koch, M. Small-Angle Scattering Studies of Biological Macromolecules in Solution. *Rep. Prog. Phys.* **2003**, *66* (10), 1735–1782.
- (114) Burrows, N. D.; Penn, R. L. Cryogenic Transmission Electron Microscopy: Aqueous Suspensions of Nanoscale Objects. *Microsc. Microanal.* **2013**, *19* (6), 1542–1553.
- (115) Patterson, J. P.; Proetto, M. T.; Gianneschi, N. C. Soft Nanomaterials Analysed by In Situ Liquid TEM: Towards High Resolution Characterisation of Nanoparticles in Motion. *Perspect. Sci.* **2015**, *6*, 106–112.
- (116) Tong, L.; Lu, E.; Pichaandi, J.; Cao, P.; Nitz, M.; Winnik, M. A. Quantification of Surface Ligands on NaYF₄ Nanoparticles by Three Independent Analytical Techniques. *Chem. Mater.* **2015**, *27* (13), 4899–4910.
- (117) Xia, X.; Yang, M.; Wang, Y.; Zheng, Y.; Li, Q.; Chen, J.; Xia, Y. Quantifying the Coverage Density of Poly(Ethylene Glycol) Chains on the Surface of Gold Nanostructures. *ACS Nano* **2012**, *6* (1), 512–522.
- (118) Maus, L.; Spatz, J. P.; Fiammengo, R. Quantification and Reactivity of Functional Groups in the Ligand Shell of PEGylated Gold Nanoparticles via a Fluorescence-Based Assay. *Langmuir* **2009**, *25* (14), 7910–7917.
- (119) Schneider, G.; Decher, G.; Nerambour, N.; Praho, R.; Werts, M.; Blanchard-Desce, M. Distance-Dependent Fluorescence Quenching on Gold Nanoparticles Ensheathed with Layer-by-Layer Assembled Polyelectrolytes. *Nano Lett.* **2006**, *6* (3), 530–536.
- (120) Valencia, P. M.; Hanewich-Hollatz, M. H.; Gao, W.; Karim, F.; Langer, R.; Karnik, R.; Farokhzad, O. C. Effects of Ligands with Different Water Solubilities on Self-Assembly and Properties of Targeted Nanoparticles. *Biomaterials* **2011**, *32* (26), 6226–6233.
- (121) Mansfield, E.; Tyner, K. M.; Poling, C. M.; Blacklock, J. L. Determination of Nanoparticle Surface Coatings and Nanoparticle Purity Using Microscale Thermogravimetric Analysis. *Anal. Chem.* **2014**, *86* (3), 1478–1484.
- (122) Wuelfing, W. P.; Gross, S. M.; Miles, D. T.; Murray, R. W. Nanometer Gold Clusters Protected by Surface-Bound Monolayers of Thiolated Poly(Ethylene Glycol) Polymer Electrolyte. *J. Am. Chem. Soc.* **1998**, *120* (48), 12696–12697.
- (123) Fabris, L.; Antonello, S.; Armelao, L.; Donkers, R. L.; Polo, F.; Toniolo, C.; Maran, F. Gold Nanoclusters Protected by Conformationally Constrained Peptides. *J. Am. Chem. Soc.* **2006**, *128* (1), 326–336.
- (124) Qian, H.; Zhu, Y.; Jin, R. Atomically Precise Gold Nanocrystal Molecules with Surface Plasmon Resonance. *Proc. Natl. Acad. Sci. U. S. A.* **2012**, *109* (3), 696–700.
- (125) De Palma, R.; Peeters, S.; Van Bael, M. J.; Van den Rul, H.; Bonroy, K.; Laureyn, W.; Mullens, J.; Borghs, G.; Maes, G. Silane Ligand Exchange to Make Hydrophobic Superparamagnetic Nanoparticles Water-Dispersible. *Chem. Mater.* **2007**, *19* (7), 1821–1831.
- (126) Torelli, M. D.; Putans, R. A.; Tan, Y.; Lohse, S. E.; Murphy, C. J.; Hamers, R. J. Quantitative Determination of Ligand Densities on Nanomaterials by X-Ray Photoelectron Spectroscopy. *ACS Appl. Mater. Interfaces* **2015**, *7* (3), 1720–1725.
- (127) Yang, J. A.; Lohse, S. E.; Murphy, C. J. Tuning Cellular Response to Nanoparticles via Surface Chemistry and Aggregation. *Small* **2014**, *10* (8), 1642–1651.
- (128) Park, J.-W.; Shumaker-Parry, J. S. Strong Resistance of Citrate Anions on Metal Nanoparticles to Desorption Under Thiol Functionalization. *ACS Nano* **2015**, *9* (2), 1665–1682.
- (129) Jackson, A. M.; Myerson, J. W.; Stellacci, F. Spontaneous Assembly of Subnanometre-Ordered Domains in the Ligand Shell of Monolayer-Protected Nanoparticles. *Nat. Mater.* **2004**, *3* (5), 330–336.
- (130) Centrone, A.; Hu, Y.; Jackson, A. M.; Zerbi, G.; Stellacci, F. Phase Separation on Mixed-Monolayer-Protected Metal Nanoparticles: a Study by Infrared Spectroscopy and Scanning Tunneling Microscopy. *Small* **2007**, *3* (5), 814–817.
- (131) Cesbron, Y.; Shaw, C. P.; Birchall, J. P.; Free, P.; Levy, R. Stripy Nanoparticles Revisited. *Small* **2012**, *8* (24), 3714–3719.
- (132) Yu, M.; Stellacci, F. Response to Stripy Nanoparticles Revisited. *Small* **2012**, *8* (24), 3720–3726.
- (133) Liu, X.; Yu, M.; Kim, H.; Mameli, M.; Stellacci, F. Determination of Monolayer-Protected Gold Nanoparticle Ligand–Shell Morphology Using NMR. *Nat. Commun.* **2012**, *3*, 1182.

- (134) Pradhan, S.; Brown, L. E.; Konopelski, J. P.; Chen, S. Janus Nanoparticles: Reaction Dynamics and NOESY Characterization. *J. Nanopart. Res.* **2009**, *11* (8), 1895–1903.
- (135) Guarino, G.; Rastrelli, F.; Scrimin, P.; Mancin, F. Lanthanide-Based NMR: a Tool to Investigate Component Distribution in Mixed-Monolayer-Protected Nanoparticles. *J. Am. Chem. Soc.* **2012**, *134* (17), 7200–7203.
- (136) Yang, J. A.; Murphy, C. J. Evidence for Patchy Lipid Layers on Gold Nanoparticle Surfaces. *Langmuir* **2012**, *28* (12), 5404–5416.
- (137) Lucarini, M.; Pasquato, L. ESR Spectroscopy as a Tool to Investigate the Properties of Self-Assembled Monolayers Protecting Gold Nanoparticles. *Nanoscale* **2010**, *2* (5), 668–676.
- (138) Dass, A.; Holt, K.; Parker, J. F.; Feldberg, S. W.; Murray, R. W. Mass Spectrometrically Detected Statistical Aspects of Ligand Populations in Mixed Monolayer $\text{Au}_{25}\text{L}_{18}$ Nanoparticles. *J. Phys. Chem. C* **2008**, *112* (51), 20276–20283.
- (139) Harkness, K. M.; Fenn, L. S.; Cliffel, D. E.; McLean, J. A. Surface Fragmentation of Complexes From Thiolate Protected Gold Nanoparticles by Ion Mobility-Mass Spectrometry. *Anal. Chem.* **2010**, *82* (7), 3061–3066.
- (140) Harkness, K. M.; Balinski, A.; McLean, J. A.; Cliffel, D. E. Nanoscale Phase Segregation of Mixed Thiolates on Gold Nanoparticles. *Angew. Chem., Int. Ed.* **2011**, *50* (45), 10554–10559.
- (141) Hu, Y.; Uzun, O.; Dubois, C.; Stellacci, F. Effect of Ligand Shell Structure on the Interaction Between Monolayer-Protected Gold Nanoparticles. *J. Phys. Chem. C* **2008**, *112* (16), 6279–6284.
- (142) Uzun, O.; Hu, Y.; Verma, A.; Chen, S.; Centrone, A.; Stellacci, F. Water-Soluble Amphiphilic Gold Nanoparticles with Structured Ligand Shells. *Chem. Commun.* **2008**, 196–198.
- (143) Stirling, J.; Lekkas, I.; Sweetman, A.; Djuranovic, P.; Guo, Q.; Pauw, B.; Granwehr, J.; Levy, R.; Moriarty, P. Critical Assessment of the Evidence for Striped Nanoparticles. *PLoS One* **2014**, *9* (11), e108482.
- (144) Ong, Q. K.; Stellacci, F. Response to Critical Assessment of the Evidence for Striped Nanoparticles. *PLoS One* **2015**, *10* (11), e0135594–19.
- (145) Marbella, L. E.; Millstone, J. E. NMR Techniques for Noble Metal Nanoparticles. *Chem. Mater.* **2015**, *27* (8), 2721–2739.
- (146) Fiurasek, P.; Reven, L. Phosphonic and Sulfonic Acid-Functionalized Gold Nanoparticles: a Solid-State NMR Study. *Langmuir* **2007**, *23* (5), 2857–2866.
- (147) Lin, W.; Insley, T.; Tuttle, M. D.; Zhu, L.; Berthold, D. A.; Král, P.; Rienstra, C. M.; Murphy, C. J. Control of Protein Orientation on Gold Nanoparticles. *J. Phys. Chem. C* **2015**, *119* (36), 21035–21043.
- (148) Whelan, D. R.; Bell, T. D. M. Super-Resolution Single-Molecule Localization Microscopy: Tricks of the Trade. *J. Phys. Chem. Lett.* **2015**, *6* (3), 374–382.
- (149) Massaro, E. S.; Hill, A. H.; Grumstrup, E. M. Super-Resolution Structured Pump-Probe Microscopy. *ACS Photonics* **2016**, *3* (4), 501–506.
- (150) Blythe, K. L.; Titus, E. J.; Willets, K. A. Objective-Induced Point Spread Function Aberrations and Their Impact on Super-Resolution Microscopy. *Anal. Chem.* **2015**, *87* (12), 6419–6424.
- (151) Lew, M. D.; Backlund, M. P.; Moerner, W. E. Rotational Mobility of Single Molecules Affects Localization Accuracy in Super-Resolution Fluorescence Microscopy. *Nano Lett.* **2013**, *13* (9), 3967–3972.
- (152) Hennig, S.; van de Linde, S.; Bergmann, S.; Huser, T.; Sauer, M. Quantitative Super-Resolution Microscopy of Nanopipette-Deposited Fluorescent Patterns. *ACS Nano* **2015**, *9* (8), 8122–8130.
- (153) ONeil, C. E.; Jackson, J. M.; Shim, S.-H.; Soper, S. A. Interrogating Surface Functional Group Heterogeneity of Activated Thermoplastics Using Super-Resolution Fluorescence Microscopy. *Anal. Chem.* **2016**, *88* (7), 3686–3696.
- (154) Willets, K. A. Super-Resolution Imaging of SERS Hot Spots. *Chem. Soc. Rev.* **2014**, *43* (11), 3854–3864.
- (155) Su, L.; Yuan, H.; Lu, G.; Rocha, S.; Orrit, M.; Hofkens, J.; Uji-i, H. Super-Resolution Localization and Defocused Fluorescence Microscopy on Resonantly Coupled Single-Molecule, Single-Nanorod Hybrids. *ACS Nano* **2016**, *10* (2), 2455–2466.
- (156) Wertz, E.; Isaacoff, B. P.; Flynn, J. D.; Biteen, J. S. Single-Molecule Super-Resolution Microscopy Reveals How Light Couples to a Plasmonic Nanoantenna on the Nanometer Scale. *Nano Lett.* **2015**, *15* (4), 2662–2670.
- (157) Silva, W. R.; Graefe, C. T.; Frontiera, R. R. Toward Label-Free Super-Resolution Microscopy. *ACS Photonics* **2016**, *3* (1), 79–86.